Title
HADRON PRODUCTION IN e+e- ANNIHILATION: QCD AND HADRONIZATION

Author
Yamamoto, H.

Publication Date
1985-12-01

Lawrence Berkeley Laboratory
UNIVERSITY OF CALIFORNIA

Physics Division

Presented at the 1985 International Symposium on Lepton and Photon Interactions at High Energies, Kyoto, Japan, August 19-24, 1985

HADRON PRODUCTION IN e^+e^- ANNIHILATION: QCD AND HADRONIZATION

H. Yamamoto

December 1985

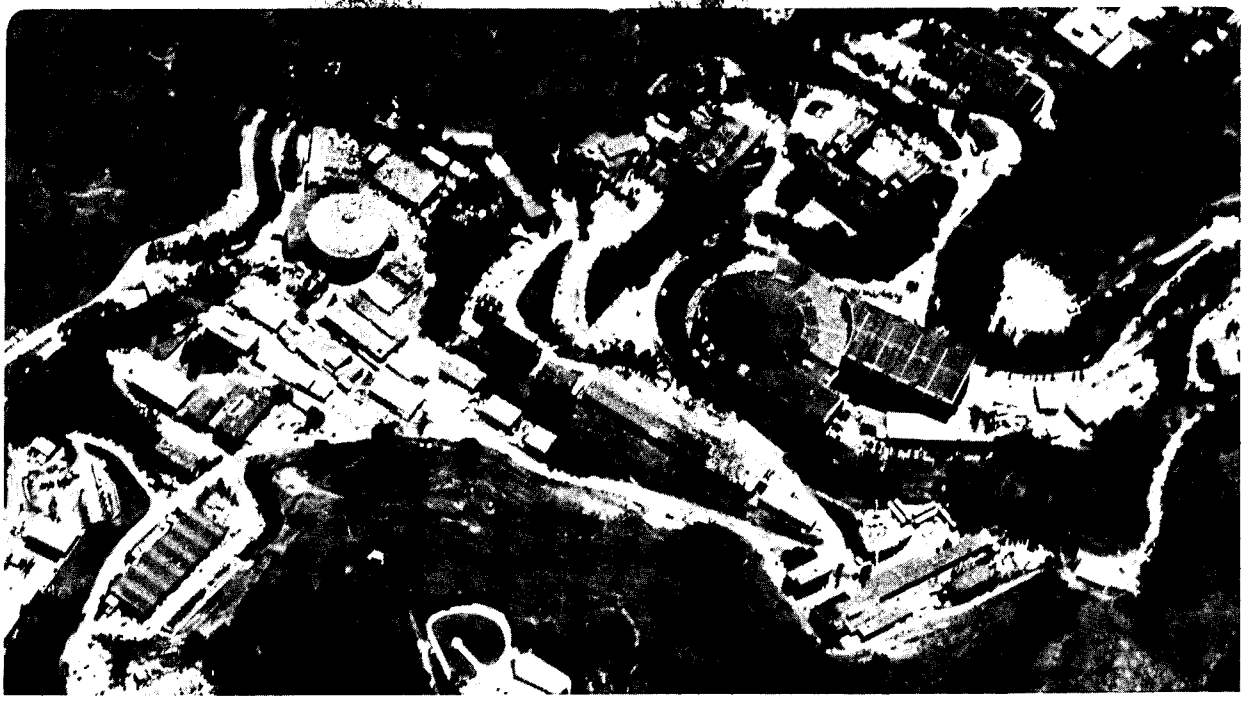

Prepared for the U.S. Department of Energy under Contract DE-AC03-76SF00098

DISCLAIMER

Hadron Production in e^+e^- Annihilation * – QCD and Hadronization –

Hiroaki Yamamoto

Lawrence Berkeley Laboratory
University of California
Berkeley, California 94720

and

Department of Physics
University of Tokyo
Hongo, Bunkyo-ku, Tokyo

Abstract

Recent results on hadron production in e^+e^- annihilation are summarized. The topics included are 1) inclusive hadron production, 2) comparison of light (u,d,s) and heavy (c,b) quark jets, 3) $p-\overline{p}$ correlations, 4) gluon vs quark jets, 5) analysis of 3 jet events, 6) measurement of the strong coupling constant α_S, and 7) forward-backward asymmetries of quarks and leptons. Experimental data are compared with predictions of several models to reveal underlying physics.

Talk presented at the
1985 International Symposium on Lepton and
Photon Interactions at High Energies
Kyoto, August 19-24, 1985

*) This work was supported by the Department of Energy under contract numbers DE-AC03-76SF00098, DE-AM03-76SF00034, and DE-AC02-76ER03330, the National Science Foundation and the Joint Japan-US Collaboration in High Energy Physics.

1 Introduction

Quantum Chromodynamics (QCD) is believed to be the fundamental theory of the strong interaction.[1,2,3] In the framework of QCD, hadron production in e^+e^- annihilation is described in the following steps:

1. Annihilation of the electron and positron into a virtual photon or Z^0.
2. Production of a quark pair with virtuality of $O(\sqrt{s})$.
3. Radiation of partons from virtual partons.
4. Hadronization of partons with low virtuality.
5. Decay of unstable particles.

In the region of large Q^2, perturbative expansion is known to work well for QCD. The steps 1) to 3) can be calculated by QCD and the Weinberg-Salam model[4] of the electro-weak interaction. In the region of small Q^2, however, QCD perturbation fails. Therefore, the hadronization of partons, step 4), is not calculable. It is not clear where the perturbative expansion breaks down, i.e., at what Q^2 value step 3) phases into step 4).

Many types of analyses have been done in e^+e^- annihilation to hadrons on each step listed above.[5,6] In the real world, the perturbative and non-perturbative phases are connected smoothly. For analysis, however, an abrupt transition between the two phases is assumed.

Perturbative calculations can only be used for partons with a virtuality above a cutoff value. Two methods exist to calculate QCD perturbatively.

A) Perturbative expansion in powers of α_S, the strong coupling constant: The cross sections for parton production in e^+e^- have been calculated up to α_S^2.[7] The results depend on the scheme used to regularize perturbative singularities. Calculations of exact matrix elements to higher orders are very difficult.

B) The Leading-collinear Logarithmic Approximation (LLA), which supplements the above exact expansion in α_S[8]: The LLA method permits emissions of as many partons as are kinematically allowed. The LLA cross sections are only approximate, however, and some cross sections are not given correctly, e.g., the 3 jet cross section with small thrust.

At the termination of the perturbative phase, the parton system must be converted to a hadronic system. At this level, the virtuality of each parton is small, the size being dependent on the cutoff. A parton at this level is not a

bare parton, but a dressed parton, i.e., a superposition of partons whose invariant mass is smaller than the Q^2 cutoff (e.g., a bare quark with acompanying collinear gluons). Several models have been proposed to describe the hadronization process based on the general arguments of QCD.[9] The most popular models are:

a) Independent Fragmentation Model (IF) (Fig.1 (a)). [10,11,12]

b) String Fragmentation Model (SF) (Fig.1 (b)).[13]

c) Cluster Fragmentation Model (CF) (Fig.1 (c)). [14,15,16]

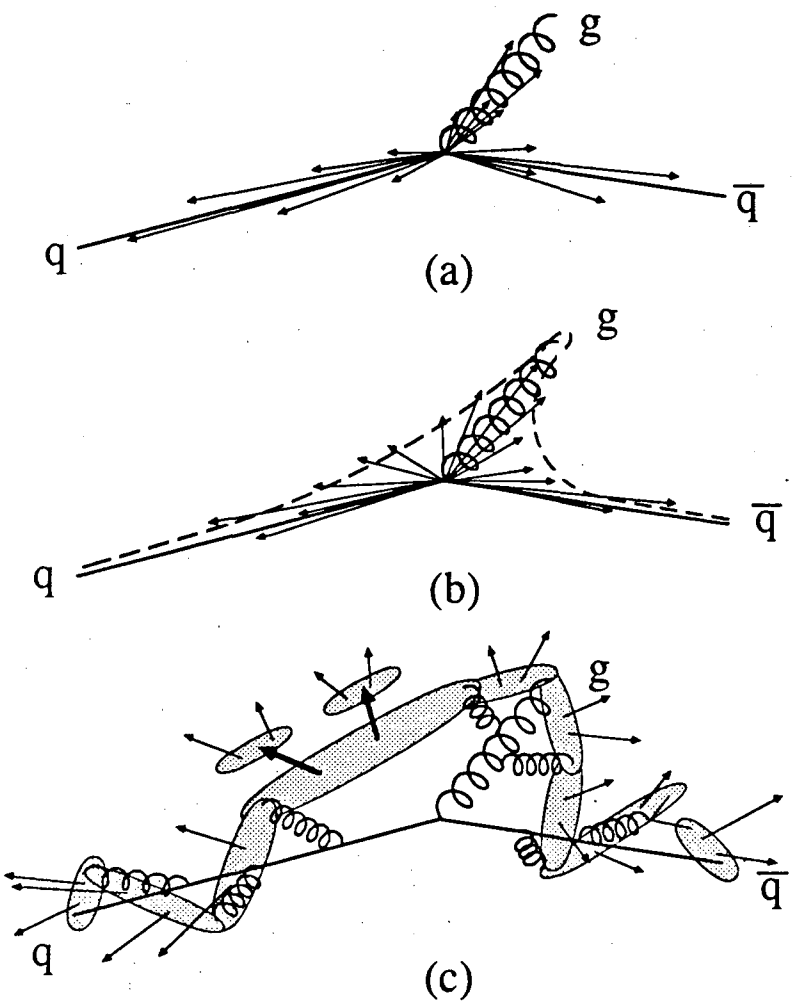

Fig. 1. Schematic representations of the 3 jet event in (a) Independent Fragmentation Model, (b) String Fragmentation Model and (c) Cluster Fragmentation Model.

The basic assumptions of these models are as follows:

a. In the IF model, each parton is assumed to fragment independently based on the Field-Feynman mechanism[10]. The hadrons produced from a parton are distributed cylindrically around the parent parton direction. A serious problem with this model is that the 4 momentum and flavor conservation is imposed in an ad-hoc manner.

b. In the SF model, it is assumed that strings are stretched between partons along the direction of color flow. This assumption is based on the string picture of confinement. Each string is assumed to hadronize with cylindrical symmetry in its rest frame. Hadrons are boosted to the e^+e^- CM frame if the CM frame and the string rest frame differ. An important consequence of this Lorentz boost is that in 3 jet events, interpreted as $q\bar{q}g$, more hadrons are produced in the regions between $q-g$ and $\bar{q}-g$ than that between $q-\bar{q}$. In this model, the 4 momentum and flavor are naturally conserved. Recent studies have shown that the hadron state produced from two partons with a small invariant mass is almost the same as the hadron state produced from a single parton with the same momentum in this model.[17] This is an attractive feature because it reduces the dependence of model predictions on the perturbative cutoff scheme.

c. The CF model is used with the LLA method. The invariant mass of two neighboring partons after the parton shower evolution by LLA is rather small, $O(1GeV)$, of the scale of hadronic masses. Based on the scheme of preconfinement, it is assumed that color singlet clusters are formed from neighboring partons. Each cluster is viewed as a heavy resonance with a large decay width. Each cluster is assumed to decay into two body states, while the flavors of the decay products are determined by their phase space and spin freedom.[18]

The IF and SF models are the two extreme cases. In the former, the interaction between partons is assumed to be negligible until the end of the hadronization process. It is clear, however, that this assumption is inapplicable for systems with small invariant mass. In the latter, maximal interaction between partons through strings is assumed. For production of hadrons with high momenta, the two models give almost the same prediction and are hardly distinguishable. The CF model where a parton shower is generated by LLA lies between IF and SF. For hadron production in the central region, it is similar to the SF model, but in the high momentum region, it predicts hadronization to proceed independently.

Questions to be addressed in the study of hadron production in e^+e^- annihilation are summarized:

1. Is the second order QCD matrix element accurate enough to describe parton production in the energy range of PEP and PETRA ? Is multi-parton production mechanism predicted by LLA necessary to explain experimental distributions ?

2. Is there a clear cutoff value of Q^2 which separates the perturbative and non-perturbative phases ? If so, what is the value ?

3. What is the difference between the quark jet and the gluon jet ?

4. Which one of IF, SF and CF is most adequate (if any) to explain parton confinement ?

In the following, experimental data are compared with several Monte Carlo predictions to test these assumptions. The principal Monte Carlo programs are:

1. The Hoyer Monte Carlo[12] and the Ali Monte Carlo[11], which uses QCD matrix element up to $O(\alpha_S^2)$ and IF.

2. The LUND Monte Carlo[13], which uses QCD matrix element up to $O(\alpha_S^2)$ and SF.

3. The Webber Monte Carlo[15] and the Gottschalk Monte Carlo[16], which use the LLA and CF. The Webber Monte Carlo, in addition, includes a part of the next leading order corrections, i.e. the soft gluon interference effect.[19]

In the following sections, recent experimental data from CESR, DORIS, PEP and PETRA are used to answer questions raised above. In Section 2, single particle production data are briefly summarized. In Section 3, light quark jets (u,d,s) and heavy quark jets (c,b) are compared to study the flavor dependence in the hadronization. Correlations between a proton and an antiproton are used to test various baryon production models in Section 4. In Section 5, gluon jets are compared with quark jets. The difference between the particle spectrum in gluon jets and that in quark jets are used to study the higher order effects neglected in the 2nd order QCD. The 3 jets events are used to evaluate the SF model and the IF model in Section 6. The effect of the soft gluon is also discussed in this section. In Section 7, the measurement of α_S is summarized. The forward-backward asymmetries of quarks and leptons are summarized in Section 8. In the last section, the summary of the talk is given.

2 Inclusive Hadron Production

The topics included in this section are: 1) multiplicities of hadrons, 2) production cross sections of charged particles with high z ($z = E_{had}/E_{beam}$), 3) charm meson production, and 4) charm baryon production.

2.1 Multiplicities of ordinary hadrons

Most low lying ordinary hadrons, which contain only u, d and s quarks, have been observed in e^+e^- experiments. These include members of the pseudo scalar and vector meson octets and of the baryon octet and decuplet. Figure 2 shows the multiplicities of ordinary hadrons measured by PEP and PETRA experiments.[20] Only those data taken in the full or nearly full momentum range are included in the figure. Recently, ARGUS has observed hyperon production at 10 GeV of Σ^*, Ξ^* and Ω^-.[21] Still remaining unobserved are η', ω, Σ and Δ. Figure 3 shows production cross sections of $K^\pm$ and Λ measured by many groups.[22] As can be seen from Fig.2 and Fig.3, data from different groups are quite consistent with few minor exceptions.

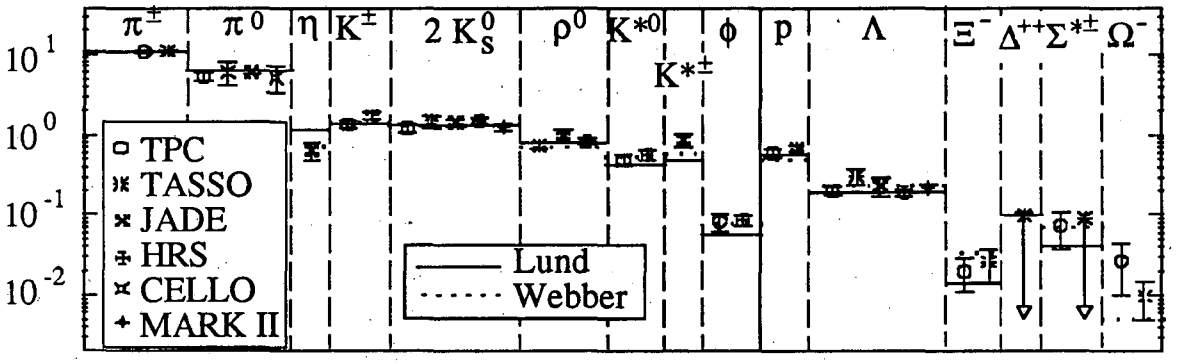

Fig. 2. Ordinary hadron multiplicities measured by PEP and PETRA experiments with Monte Carlo predictions.

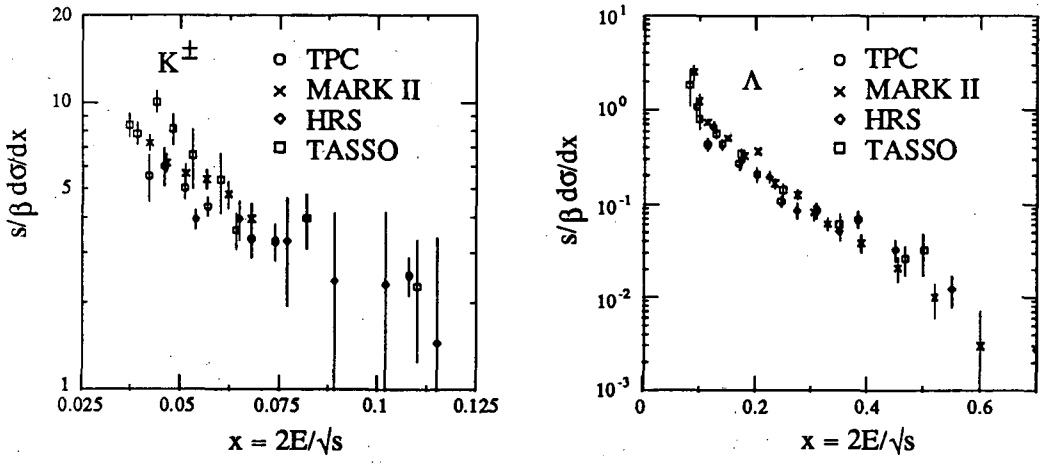

Fig. 3. Inclusive cross sections of $K^\pm$ and Λ at PEP and PETRA.

In Fig.2, the predictions of the Lund SF and Webber CF models are also shown. The two models are in reasonable agreement with observed multiplicities and single particle cross sections, despite the very different manners in which the relative abundance and the spectrum shape are determined.

In the Lund model, the production rate of a hadron with a given flavor is mainly determined by the rates of quark-antiquark and diquark-antidiquark pair produced in the string-like color field. The physical motivation comes from 2-dimensional field theory, but several phenomenological parameters have been introduced, which are to be determined by experimental data. For example, the s/u ratio (ratio of $s\bar{s}$ to $u\bar{u}$ pair production rates) is determined from the ratio of multiplicities for kaons and pions. The momentum spectrum is determined by the fragmentation function of quarks.[23]

In the Webber model, the differential cross section is determined in two steps. First, parton configurations are generated in momentum space in LLA, and the mass and momentum of color singlet clusters are determined. Next, these clusters decay to hadrons governed only by kinematical factors, i.e., phase space and spin factors.

2.2 Charged Particle Cross Section at high z

The charged particle cross section in the high z region ($z = E_{had}/E_{beam}$) has been measured by HRS at PEP.[24] (Fig.4) The cross section in this region is very interesting because 1) the contribution of the decay products from resonant particles is small, and 2) the behavior of the cross section is strongly model dependent at around $z = 1$. Such a measurement is only possible with their good momentum resolution, $\Delta p/p = 0.25\% p(GeV/c)$ at $p_{had} = E_{beam}$. The number of background events above $z = 0.9$ is estimated to be less than 0.1.

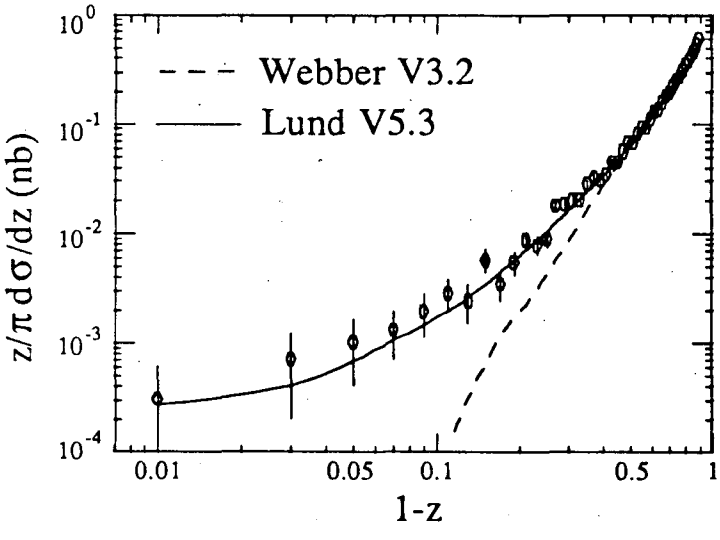

Fig. 4. HRS date of the charged particle cross section at high z with Monte Carlo predictions.

In Fig.4, the predictions of the LUND MC and the Webber MC are also shown. As can be seen, the LUND MC gives a good description of the data, but the Webber MC predicts too soft a momentum spectrum above $z = 0.6$. In order to trace back the origin of this problem in the Webber MC, another combination of assumptions was tested in which the perturbative phase is based on LLA (as before) but the hadronization phase is based on SF. This model gives almost the same result as the LUND MC. Failure of the Webber MC in the high z region is now explained by the fact that the cluster is forced to decay into two hadrons. It is then difficult to produce a high z hadron, even if the energy of the cluster is approximately equal to the beam energy. This difficulty is common to hadronization scheme based on cluster decay. If a cluster with small invariant mass is replaced by a hadron with a mass close to the cluster mass, the predicted spectrum becomes harder.[25]

2.3 Charm meson production

The $D^{*\pm}$ provides a unique tool for measuring the fragmentation function of c quark. The $D^{*\pm}$ cross sections measured by DELCO, HRS, TPC, JADE and TASSO at around $E_{CM} = 30\ GeV$ are shown in Fig.5(a).[26] The D* cross sections measured at different E_{CM} are compared in Fig.5(b), DELCO at 29 GeV, CLEO and ARGUS at 10 GeV and MARK I at 7 GeV. Here the data by MARK I is the D cross section. The cross section $s \cdot d\sigma/dx$ is almost independent of E_{CM}. The absolute value of the production cross section depends on the branching fractions of the D meson. In this regard, the fact that the latest MARK III data[27] significantly differs from the values in the Particle Data Table[28] has effects on the production cross section. The cross section given here will become smaller if the new branching fractions are used. The spectrum is harder for D* than that for ordinary hadrons.

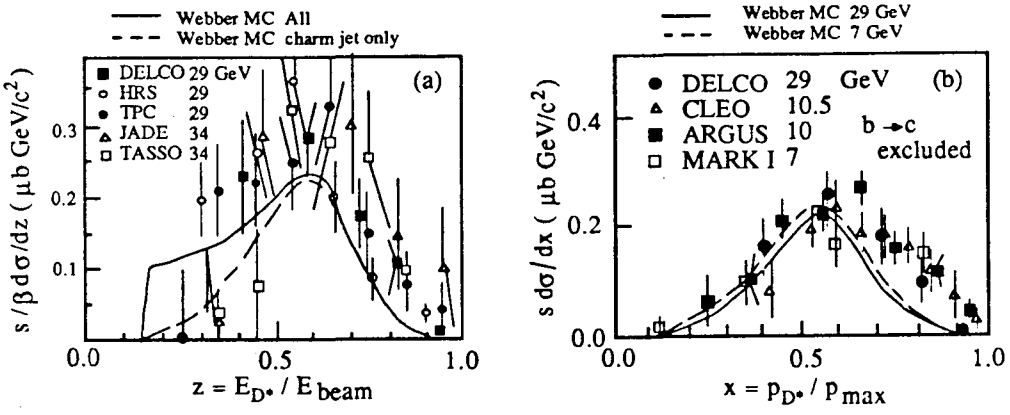

Fig. 5. Cross sections of D* measured at PEP, PETRA, CESR, DORIS and SPEAR.

The observed hadron spectrum deviates from the fragmentation function at the parton level due to radiative corrections, multi-jet emissions and kinematics. These effects have been analized by Bethke. Comparison of the observed $< x >$ and the corrected $< z >$ after unfolding these effects is shown in Fig.6.[29] As can be seen from this figure, $< z >$ is almost independent of E_{CM} in the range of $10 - 34\ GeV$. The average value of z was found to be $0.71 \pm 0.014 \pm 0.03$.

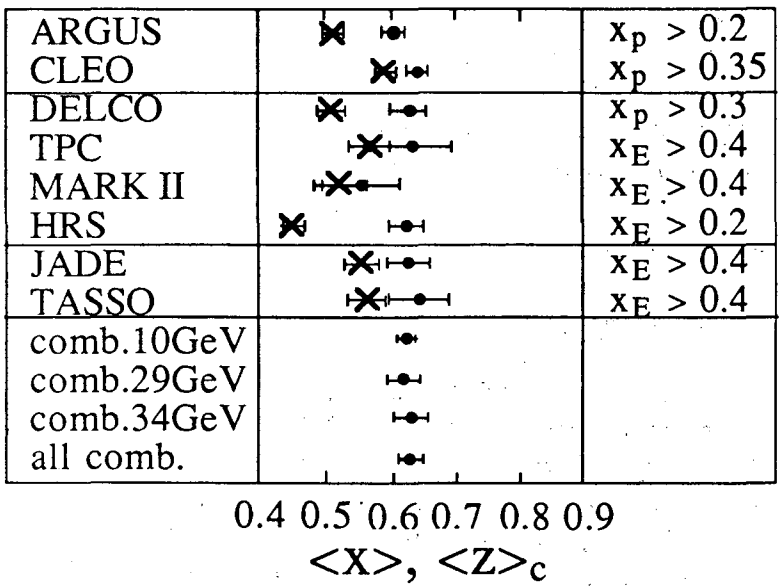

Fig. 6. Average value of the scaled momentum of D* before ($< x >$, marked by cross) and after ($< z >$, marked by circle) corrections mentioned in the text.

In Fig.5(a) and (b), predictions of the Webber MC are also shown. In the Webber model, the fragmentation function is not given externally but is determined by dynamics (LLA) and kinematics (masses of quarks and hadrons). The flavor dependence of the inclusive spectrum comes mainly from differences in quark mass. The Webber MC predicts too soft a spectrum in the high z region, but the spectrum around $z = 1$ depends strongly on the assumption made for the production of heavier resonances, e.g., D**.

2.4 Charm baryon production

New observations of Λ_c production in e^+e^- annihilation have been reported by CLEO[30] ($\Lambda_c \to \Lambda\pi\pi\pi$) and ARGUS (preliminary)[21] ($\Lambda_c \to pK\pi$). The CLEO data were taken on, just below, and above the $\Upsilon(4)$ mass. The contribution from B meson decay are found to be negligible in this region. The ARGUS data were taken on and off the 4 Υ resonances. No significant difference was observed between the Λ_c signals on and off resonances in the ARGUS data, and the Λ_c production rate in the Υ decay is smaller than the Λ_c production rate in charm jets. The invariant mass distributions are shown in Fig.7(a) and (b). The observed Λ_c masses are $2.287 \pm 0.011 \pm 0.005\ GeV$ (CLEO) and $2.284 \pm 0.0035 \pm 0.0021\ GeV$ (ARGUS).

The cross sections are shown in Fig.8 as a function of scaled momentum. The solid line in this figure is the Peterson function[32] with $\epsilon = 0.14$, fitted to the D* spectrum obtained by CLEO. The best fit of ϵ for Λ_c by CLEO and by ARGUS are 0.21 ± 0.08 and $0.172\ ^{+0.128}_{-0.088}$, respectively. No significant difference is observed between the charm meson spectrum and the charm baryon spectrum.

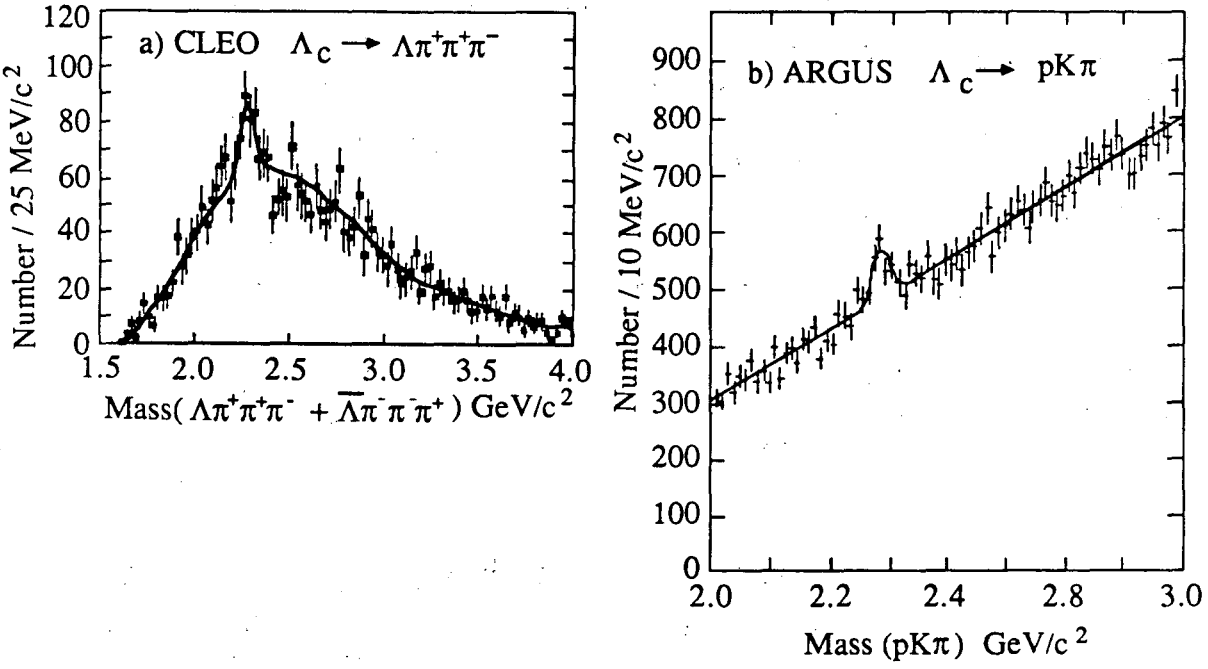

Fig. 7. Invariant mass distributions of $\Lambda\pi\pi\pi$ and $pK\pi$ measured by CLEO and ARGUS.

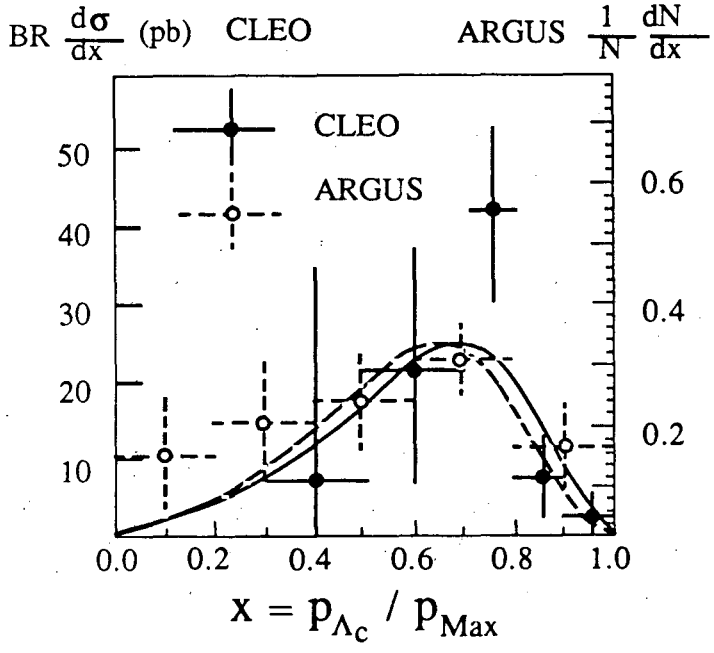

Fig. 8. Momentum distribution of Λ_c measured by CLEO and ARGUS. The solid line is the Peterson function fitted to CLEO D* data and the broken line is the same function fitted to the ARGUS data.

CLEO obtained the expected number per event for $e^+e^- \rightarrow \Lambda_C + X$ followed by $\Lambda_C \rightarrow \Lambda\pi\pi\pi$ to be $0.0044 \pm 0.0011 \pm 0.0015$. According to MARK II[31], 0.2 Λ_C's are produced per c quark. Using this, CLEO found the branching fraction for $\Lambda_C \rightarrow \Lambda\pi\pi\pi$ to be $2.8 \pm 0.7 \pm 1.1\%$. ARGUS found the total cross section to be $859 \pm 164^{+716}_{-269}$ pb from $\sigma \cdot BR = 18.9 \pm 2.3 \pm 2.7$ pb. Using this cross section, they found the ratio of Λ_C to $D^{*\pm}$ production rates to be $0.98 \pm 0.31^{+0.8}_{-0.3}$.

All Monte Carlo programs predict the charm baryon spectrum to be similar to the charm meson spectrum in shape, and this prediction is consistent with data. The comparison of the absolute production rate between the model prediction and the data is difficult because branching fractions are not well known for most decay modes.

3 Flavor dependence of Jets – u,d,s vs c,b jets

The flavor dependence of the hadronization process has been tested using events tagged by large p_t leptons or D*. In this section, the following topics are covered: 1) hadron multiplicities, 2) p and p_t distributions and 3) α_S in heavy quark jets.

3.1 The multiplicities in heavy quark jets

The total multiplicity in $Q - \overline{Q}$ jets (Q = c or b quark) is the sum of two components; 1) the decay products of the heavy hadron which contains Q or $\overline{Q}$ (leading part) and 2) the hadrons which are produced from the non-leading part of jets. The multiplicity of non-leading part is denoted N_{NL}. The question raised here is whether the non-leading part depends on the flavor of the leading quark Q.

MARK II used leptons to enrich c and b jets by requiring $p \geq 2GeV/c$ and $p_t < 1\ GeV/c$ (for charm), and, $p \geq 2\ GeVc$ and $p_t \geq 1\ GeV/c$ (for bottom).[33] The average total charged multiplicities in $Q - \overline{Q}$ jets obtained in this analysis are $16.1 \pm 0.5 \pm 1.0$ for bottom events and $13.2 \pm 0.5 \pm 0.9$ for charm events. The non-leading hadron multiplicity N_{NL} has been estimated by subtracting the average multiplicity of the leading part from the total multiplicity; $N_{NL}(bottom) = 5.2 \pm 0.5 \pm 0.9$ and $N_{NL}(charm) = 8.1 \pm 0.5 \pm 0.9$. The average invariant mass of the non-leading part, W_{NL}, and the mean energy fraction of the heavy hadron $< z >_Q$ are related by the following equation:

$$W_{NL} = E_{CM} \cdot (1 - 2 \cdot < z >_Q).$$

In Fig.9, the average charged multiplicity over a wide range of E_{CM} are shown. Assuming that the relation between N_{NL} and W_{NL} is the same as that between the average charged multiplicity and E_{CM}, they found the mean

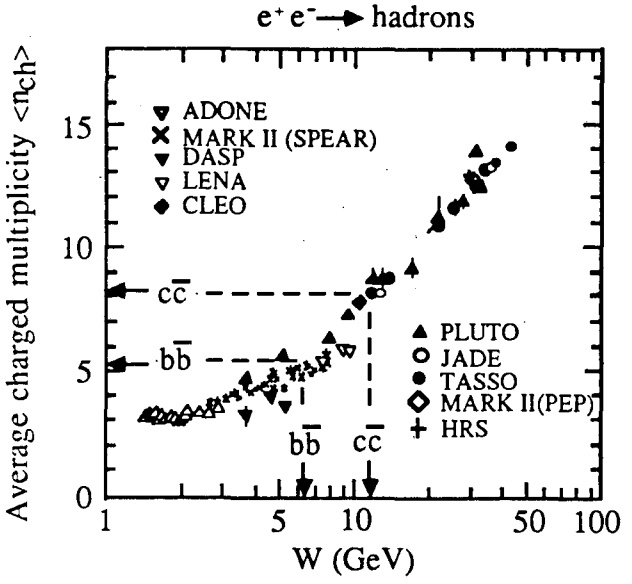

Fig. 9. The energy dependence of the charged multiplicity in e^+e^- annihilation. The arrows indicate the non-leading charged multiplicities for $b\bar{b}$ and $c\bar{c}$ events, and the corresponding invariant masses.

energy fraction of heavy hadrons $< z >_Q$ to be $< z >_b = 0.79^{+0.10}_{-0.05}$ and $< z >_c = 0.60^{+0.09}_{-0.11}$. These values are consistent with measurements based on lepton inclusive spectra and D* fragmentation.[26,33,34] Turning the argument around, one can conclude that the hadronization of the non-leading part is independent of the leading flavor.

3.2 Inclusive momentum distribution

Several groups have studied particle distributions in the side of the event opposite to side of the particle used to tag the specific quark type. In this subsection, the results reported by HRS (preliminary) for light quark jets vs charm jets[35], and by DELCO for average jets vs bottom jets[36], are presented.

HRS has used large momentum charged particles to tag light quark jets. They required the existence of charged particles with z larger than 0.7. The charm events are tagged by observing a peak in the D*-D mass difference, with an assumed D decay mode of $D \to K\pi$ and $D \to K\pi\pi\pi$. For the 1st decay mode, the minimum z is required to be 0.4, for the 2nd it is required to be 0.5. The purity of the light quark jet sample is estimated to be 89%, and that of the charm quark jet sample to be 85 %. The absolute momentum and transverse momentum distributions are shown in Fig.10(a) and (b). The average values are summarized in Table 1.

DELCO has used electrons with $p = 0.5 - 5.5 GeV$ and $p_t > 1 GeV$ to tag bottom quark jets, and has compared those jets with jets in the their entire event sample. The estimated purity of the bottom jet sample is 83 %. The rapidity

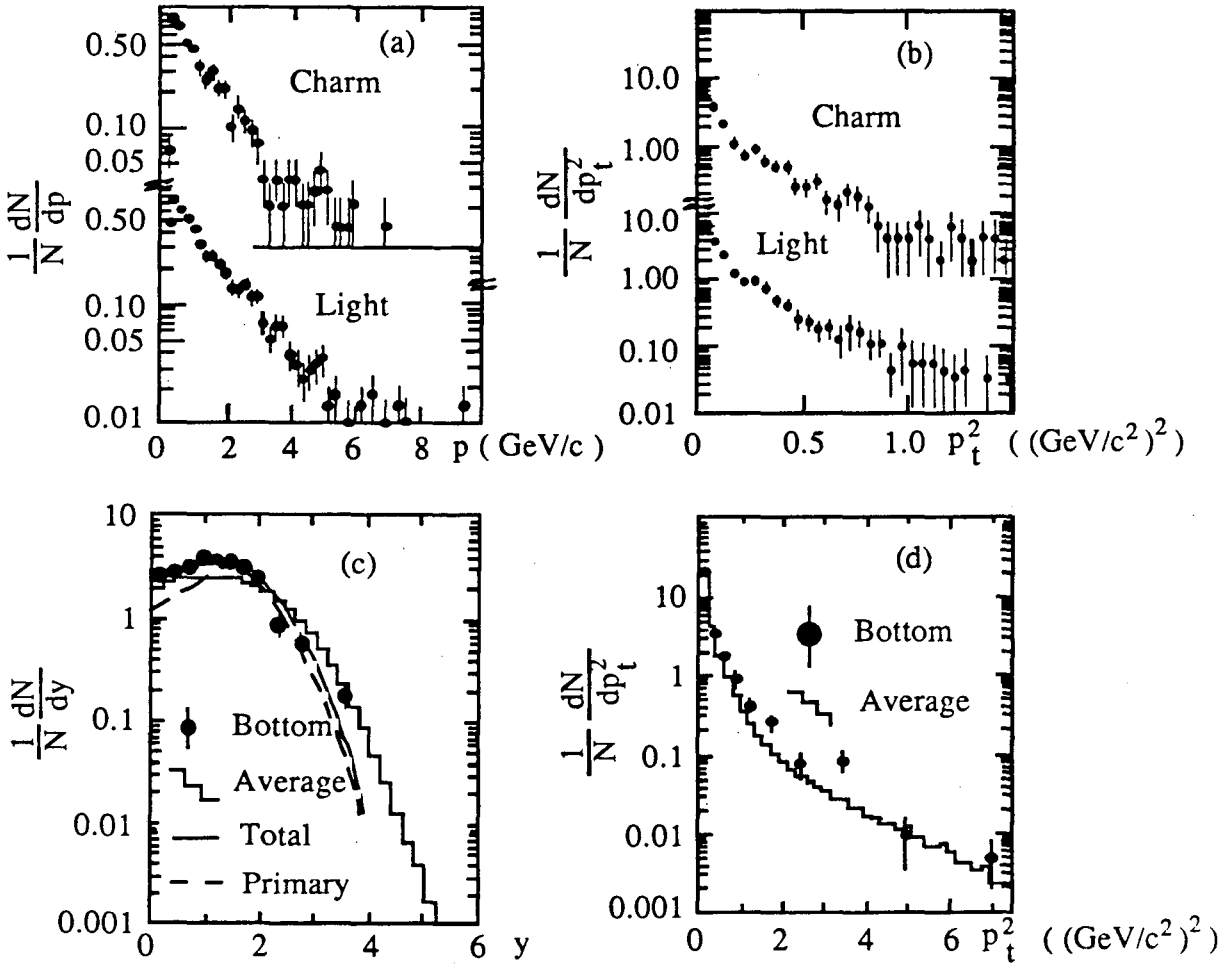

Fig. 10. Charged particle distribution in charm and light jets measured by HRS ((a), (b)), and, that in bottom and average jets measured by DELCO ((c) and (d)). The LUND MC predictions are given in (c) for total and for primary hadrons.

	HRS		DELCO	
parameters	charm	light	bottom	average
$< N_{h^\pm} >$	6.6±0.2	5.8±0.1	7.61±0.46	6.16±0.01
$< p >$	1.38±0.06	1.52±0.04	1.06±0.04	1.293±0.002
$< y >$			1.20±0.03	1.400±0.002
$< p_t >$	0.39±0.01	0.40±0.01		
$< p_t^2 >$			0.31±0.03	0.274±0.001
$< S >$	0.094±0.010	0.087±0.007	0.26±0.02	0.141±0.001
$1- < T >$	0.082±0.005	0.092±0.004	0.149±0.009	0.1060±0.0003

Table 1. Average values of event parameters. Errors are statistical only.

and p_t distributions are shown in Fig.10(c) and (d). The average values are summarized in Table 1.

No significant difference is observed between charm quark jets and light quark jets, except that the average momentum in charm jets is slightly softer than that in light quark jets. This result can be reproduced by models where same hadronization scheme is used for light quark jets and charm quark jets. The observed rapidity distribution in the bottom quark jet is slightly softer than that in the average jets, and shows a dip at $y = 0$. In Fig.10(c), the LUND Monte Carlo predictions are shown, in which the hadronization process is the same for all types of quark jets. The solid line shows that of all particles and the broken line shows the rapidity distribution of the leading hadrons. The leading hadron distribution gives a clear dip at $y = 0$ due to kinematics, the large $< z >$ of bottom hadrons and subsequent decays with high multiplicity. The solid line is consistent with data and the difference between the bottom jet and the average jet can be explained by the difference in the leading hadrons.

3.3 α_S measured in heavy quark jets

In QCD, α_S is assumed to be flavor independent. The test is made in e^+e^- experiments by using charm events tagged by D*. Discussions on α_S in average events will be given in Sec.7.

TASSO obtained α_S using the distribution of p_t of charged particles in the event plane.[37] They found $\alpha_S(c) = 0.153 \pm 0.031 \pm 0.030$ in charm quark jets using IF models for hadronization with 2nd order QCD calculation for the parton cross section. They also obtained the ratio of α_S in charm quark jets and in average jets: $\alpha_S(c)/\alpha_S(average) = 1.00 \pm 0.20 \pm 0.20$.

JADE used eigenvalues Q_i (i=1,2,3 and $Q_1 < Q_2 < Q_3$) of the normalized sphericity tensor to obtain $\alpha_S(c)$.[38] They found the fraction of planar events ($Q_3 < 0.9$, $Q_1 < 0.06$) to be 13 ± 4 % for the charm events and 10 ± 1 % for all events with at least one charged particle with $z > 0.4$. The requirement of a large momentum charged track is to make the kinematical coniditions of average events similar to that of tagged events. From these fractions, they obtained $\alpha_S(c) = 0.13 \pm 0.08$ using the LUND MC.

HRS tagged light quark jets by requiring large momentum charged particles as mentioned in Sec.3.2. They selected 3 jet and 2 jet events using the invariant mass of jets. From the ratio of the number of 3 jet events to the number of 2 jet events in tagged light quark events and in tagged charm quark events, they obtained the ratio $\alpha_S(c)/\alpha_S(u,d,s) = 1.03 \pm 0.27$ (preliminary).[39] It is assumed that the ratio of 3 jet to 2 jet events is proportional to α_S. The quoted errors are statistical only.

The α_S measured for charm quark is equal to α_S measured for average quarks (see Sec.7) within statistics and no flavor dependence is observe.

4 $p-\overline{p}$ correlations and the baryon production mechanism

The study of correlations between hadrons provides information which is unattainable from single particle inclusive analysis. For example, the correlation between charged particles with the same sign provides information about the spatial extent of hadron sources (GGLP effect).[40] Presented in this section is the analysis of $p-\overline{p}$ correlations performed by TPC to study the baryon production mechanism.[41] TPC examined two distributions:

1. The angular distribution of baryon production relative to the jet axis.
2. The strength of the transverse momentum correlation between the two members of a baryon-antibaryon pair.

The first distribution was used to test the cluster decay model and the string model diquark mechanism. The second distribution was used to study diquark model and the so-called "popcorn" model.

4.1 Models for baryon production

Several mechanisms for baryon production in e^+e^- annihilations have been proposed. The major models are 1) the diquark model[42] (Fig.11(a)), 2) the popcorn model[43] (Fig.11(b)), and 3) the cluster decay model[44] (Fig.11(c)). In the diquark model, the diquark is considered to be a (effectively) fundamental "particle". The diquark-antidiquark pair is produced from the color field like an ordinary quark-antiquark pair. A baryon is produced by combining a diquark and a quark. The popcorn model was introduced in order to explain baryon production in QCD. In this model, only quark pairs are produced from the color field. It was shown that three quarks can combine themselves to form a color singlet system with a reasonable rate. In the cluster decay model, a baryon pair is produced through the decay of clusters in the same way as a meson pair. In the Webber model, gluons split into quark-anitquark pairs and only mesonic clusters (cluster which contain a quark and an antiquark) appear. A cluster is assumed to decay isotropically into two hadrons in the rest frame of the cluster.

4.2 Cluster decay vs String Model

TPC obtained 110 $p\overline{p}$ and 21 pp, $\overline{p}\overline{p}$ pairs in the proton momentum range of 0.5 to 1.5 GeV, with estimated background of 7 and 3, respectively. In order to see how the cluster decay model differs from other two models, the angular distribution of $p\overline{p}$ pairs with respect to the jet axis was studied. The angle θ^* is defined as the angle between the proton momentum and the jet

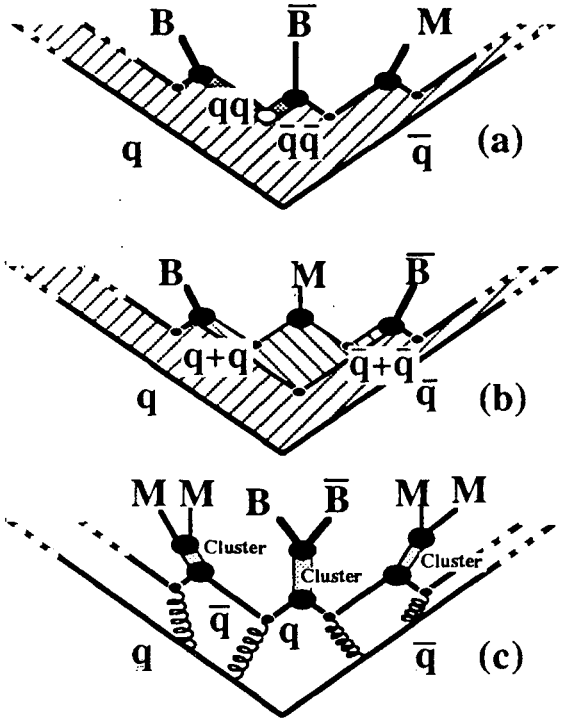

Fig. 11. Schematic representation of baryon production mechanisms in (a) diquark model, (b) "popcorn" model and (c) cluster decay model.

axis in the CM frame of the $p\overline{p}$ pair. In the cluster decay model, the cluster decays spherically symmetric and the $\cos\theta^*$ distribution is flat. In the diquark model, the proton and antiproton are more likely to be produced along the jet direction because the diquarks are pulled along the direction of the string. The popcorn model gives almost the same prediction as the diquark model in this distribution. The θ^* distribution in the diquark model shows an enhancement around $|\cos\theta^*| = 1$. In order to remove the contributions of $p\overline{p}$ pairs in which the p and $\overline{p}$ are produced independently, the θ^* distribution is defined as follows;

$$dn/d|\cos\theta^*| = dn/d|\cos\theta^*|(p+\overline{p}) - dn/d|\cos\theta^*|(p+p, \overline{p}+\overline{p}) \ ,$$

where $dn/d|\cos\theta^*|(p+\overline{p})$ is the distribution of the $p\overline{p}$ pairs and $dn/d|\cos|(p+p, \overline{p}+\overline{p})$ is that of the pp and $\overline{p}\overline{p}$ pairs.

The $|\cos\theta^*|$ distribution measured by TPC is shown in Fig.12 together with the predictions of the diquark model and the cluster decay model. The shape of the distributions suffer from the limited momentum range of p and $\overline{p}$, but the relative difference between the two models is retained. As can be seen from the figure, the data shows an enhancement around $|\cos\theta^*| = 1$. The diquark model reproduces this shape. The cluster decay model, however, shows a decrease at $|\cos\theta^*| = 1$ and is excluded at 95% CL.

The above result means that baryon pairs are oriented primarily along the jet axis a *la* diquark model prediction and that the the baryon pairs are not

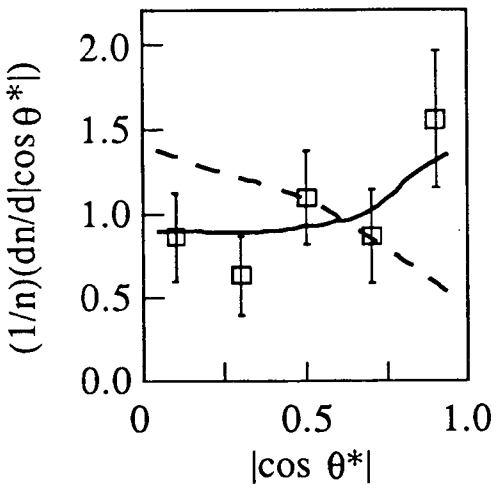

Fig. 12. Distribution of $p-\bar{p}$ pairs in θ^* with predictions of the LUND diquark model (solid line) and of the Webber MC (dahsed line).

produced isotropically in the CM frame of the pair. The implication for the Webber model is that either baryonic clusters, i.e. clusters which contain three quarks, must be introduced or that clusters must decay anisotropically. An updated version of Webber MC (V3.2), which includes baryonic clusters by allowing the splitting of virtual gluons into diquarks, reproduces the enhancement at $|\cos\theta^*| = 1$.

4.3 Diquark model vs Popcorn model

In the diquark model, the baryon and antibaryon are always adjacent, while mesons can be produced between the baryon and antibaryon in the popcorn model. Because of this difference, the correlation between the p and $\bar{p}$ momentum transverse to the jet axis is stronger in the diquark model than that in the popcorn model. To measure the strength of this correlation, the following quantity α is defined using the transverse momenta of the proton $\vec{p_t}(p)$ and the antiproton $\vec{p_t}(\bar{p})$;

$$\alpha \equiv < \vec{p_t}(p) \cdot \vec{p_t}(\bar{p}) > / < \vec{p_t}(p)^2 > .$$

The diquark model predicts $\alpha = -1/2$ at the generator level. In the real analysis, several effects smear this prediction. The largest effect is hard gluon emission. Because of hard gluon emission, the jet axis (sphericity axis) is not the direction of the quark or gluon. To make the analysis less dependent on the gluon emission, α_{out} is defined from the same equation by using the transverse momentum component out of the event plane.

In order to simulate the popcorn model, a simple mechanism has been incorporated into the LUND MC, whereby baryon pairs are produced with or without a meson between the baryon and the antibaryon.[43] The ratio $BM\overline{B}/(BM\overline{B} +$

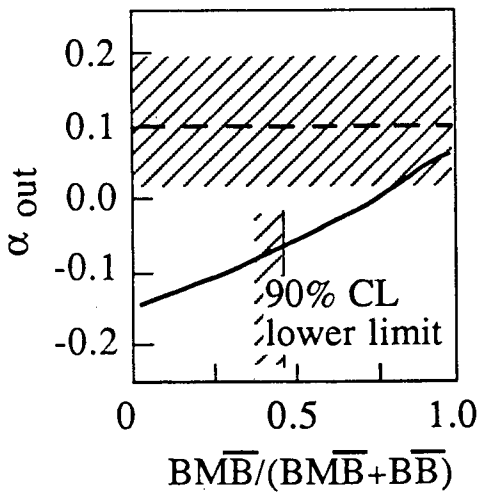

Fig. 13. Correlation coefficiant α_{out} with the popcorn model prediction as a function of the fraction $BM\overline{B}/(B\overline{B}+BM\overline{B})$.

$B\overline{B}$) is defined as the fraction of baryon pairs with such an intermediate meson. The prediction with $BM\overline{B}/(BM\overline{B}+B\overline{B})=0$ corresponds to the diquark model.

The measured α_{out} is shown in Fig.13. The data shows a very weak correlation between the transverse momentum of the proton and that of antiproton. In the same figure, the prediction of the popcorn model is shown as a function of $BM\overline{B}/(BM\overline{B}+B\overline{B})$. This prediction is insensitive to the perturbative part, i.e., the result is almost the same for 2nd order QCD and for the LLA. From this data, the lower limit on the fraction $BM\overline{B}/(BM\overline{B}+B\overline{B})$ was calculated to be 45% at 90% CL.

5 Gluon vs Quark Jet

In this section, gluon jets are compared with quark jets. The topics covered are: 1) baryon multiplicities in gluon jets and 2) the momentum spectra of particles in gluon jets vs quark jets.

5.1 Baryon multiplicities

Since the discovery of gluon jets at PETRA, comparisons between gluon and quark jets have been made extensively.[6] One interesting difference is the observation of more baryons in gluon jets than in quark jets. Several groups have reported recently on this issue. Figure 14 shows some of the results, by (a) TASSO, (b) MARK II and (c) HRS.

TASSO reported the observed multiplicity of Λ in 2 and 3 jet events as a function of the jet energy.[45] They compared data with MC predictions assuming several different ratios for the baryon multiplicities in gluon jets and in quark

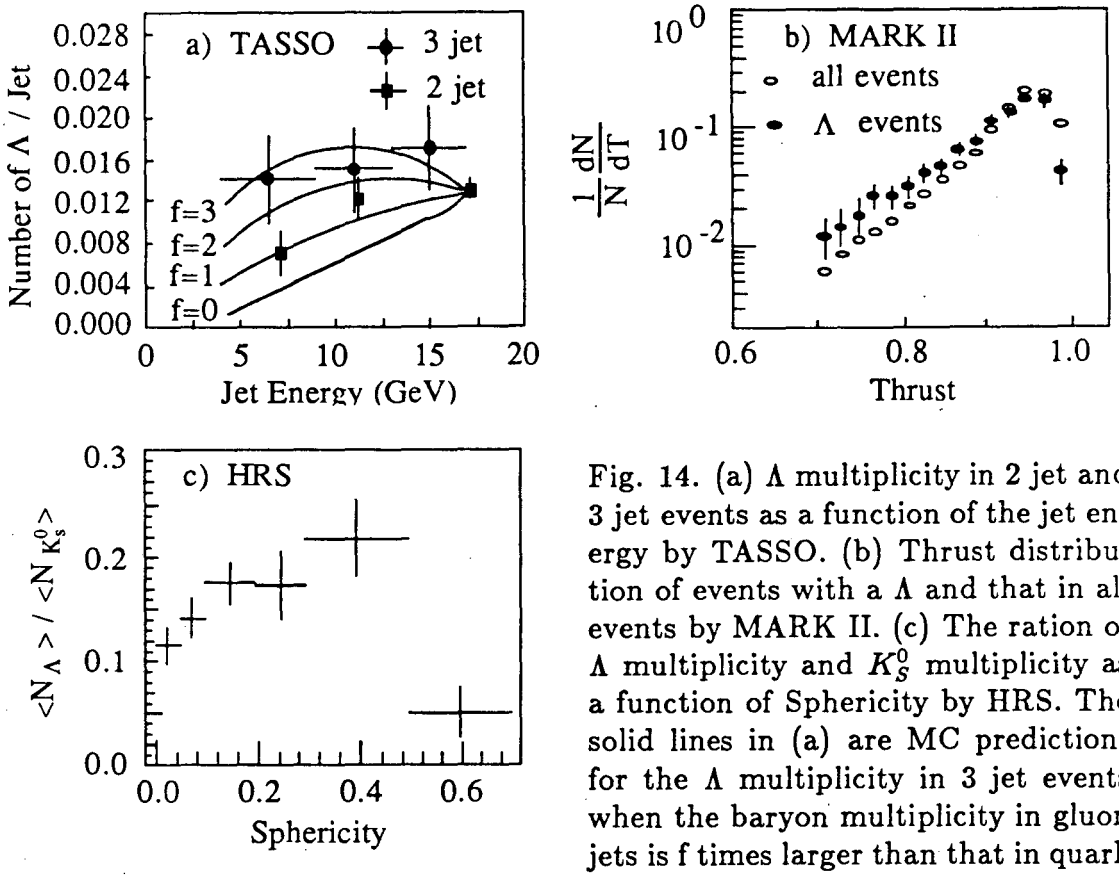

Fig. 14. (a) Λ multiplicity in 2 jet and 3 jet events as a function of the jet energy by TASSO. (b) Thrust distribution of events with a Λ and that in all events by MARK II. (c) The ration of Λ multiplicity and K^0_S multiplicity as a function of Sphericity by HRS. The solid lines in (a) are MC predictions for the Λ multiplicity in 3 jet events when the baryon multiplicity in gluon jets is f times larger than that in quark jets.

jets. This study indicates that the baryon multiplicity is larger in gluon than that in quark jets. MARK II compared thrust distribution for events which contain a Λ with that for all events.[46] HRS gave the ratio of the baryon and meson production rates as a function of sphericity.[47]

All these results are consistent with the assumption of higher baryon multiplicity in gluon jets relative to quark jets. Further study is required, possibly by comparing the data for hadron production on and off the Υ resonance.[48]

5.2 Hadron spectrum in gluon jets and quark jets

The particle momentum spectra in gluon jets and in quark jets have been compared by MARK II.[49] The analysis uses charged particles and photons in 90000 events and proceeds as follows:

- 3 jet events are selected by using a cluster algorithm.
- The momentum of each jet is calculated by summing the momentum vector of particles which belong to the jet. The energy of the jet is calculated

from opening angles between jets assuming massless parton kinematics.

- Events with a nearly 3-fold symmetry are selected by requiring the opening angles between any two jets to lie between 100° and 140°. Total of 560 events are selected to be used in the following analysis.

- The scaled momentum of each particle is defined to be $x_i = p_i/E_j$, where p_i is the momentum of particle i and E_j is the energy of the jet to which it is assigned.

- The distribution in x is corrected for the detector acceptance and initial state radiation. This momentum distribution is viewed as the sum of the distributions in one gluon jet and two quark jets with energy of $1/3E_{CM}$ each.

- The momentum distribution in events with two quark jets of energy $1/3E_{CM}$ each is calculated by interpolation of existing data at several different energies. Most events in these samples are 2 jet events and can be used to approximate the particle distribution for 2 jet events. The broken line in Fig.15(a) is the distribution obtained by this interpolation.

- The scaled momentum distribution in gluon jets is calculated by the following equation.

$$\begin{aligned} \frac{1}{\sigma_{tot}}\frac{d\sigma}{dx}(gluon\ jet) &= \frac{1}{\sigma_{tot}}\frac{d\sigma}{dx}(3\ jet\ events, E_{CM} = 29GeV) \\ &- \frac{1}{\sigma_{tot}}\frac{d\sigma}{dx}(2\ jet\ events, E_{CM} = 19.3GeV) \end{aligned}$$

- The ratio $r(x)$, which approximates the ratio of $\frac{1}{3}(gluon\ jet + 2 \cdot quark\ jet)\ /\frac{1}{2}(2 \cdot quark\ jet)$, is defined as follows

$$r(x) = \frac{\frac{1}{3\sigma_{tot}}\frac{d\sigma}{dx}(3\ jet\ events, E_{CM} = 29GeV)}{\frac{1}{2\sigma_{tot}}\frac{d\sigma}{dx}(all\ events, E_{CM} = 19.3GeV)}$$

Figures 15(a) and (b) show the results for $1/\sigma_{tot} \cdot d\sigma/dx(gluon\ jet)$ and $r(x)$, respectively, along with the predictions of several Monte Carlo programs. In Fig.15(a), black circles denote the distribution of particles in 3 jet events, while the white circles correspond to the distribution in gluon jets defined above. By comparing the broken line and the distribution in gluon jets, it is observed that the spectrum is softer in gluon jets than that in quark jets. The same conclusion can be reached in Fig.15(b).

The LUND and Ali MC's give too hard a spectrum in gluon jets, while that the Webber MC gives fairly good description of the data, as seen in Fig.15(b). Further study has been made on this subject by using different kinds of MC's.

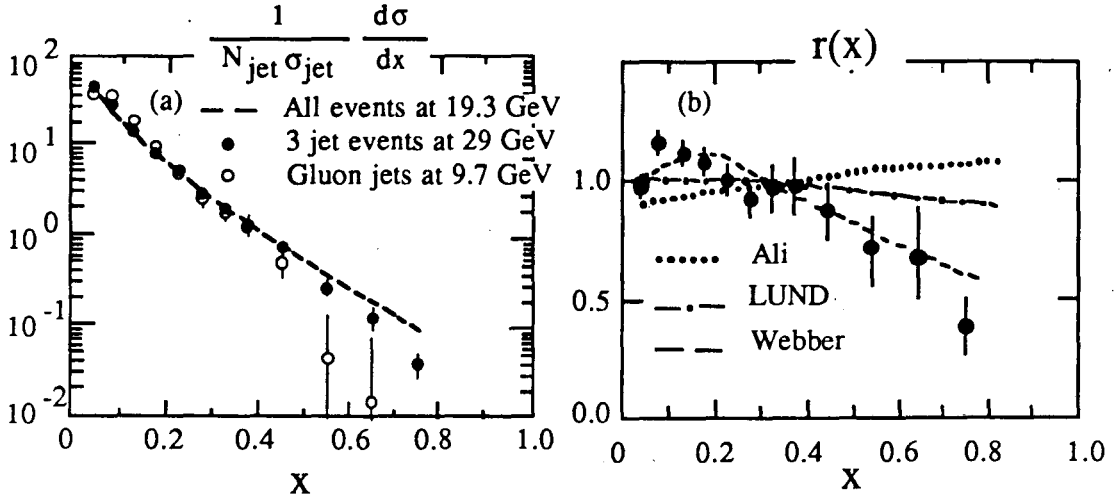

Fig. 15. (a) The charge particle distribution in 3-fold symmetric 3 jet events in comparison with that in hadronic events at 9.7 GeV. The distribution in gluon jets at 9 GeV mentioned in the text is shown by open circles. (b) The ratio $r(x)$ defined in the text as a function of x, with several Monte Carlo predictions.

1) 2nd order QCD + SF with m fixed, where m is the minimum invariant mass of two partons.

2) 2nd order QCD + SF with y fixed, where $y = m^2/E_{CM}^2$.

3) LLA + CF.

4) LLA + SF.

5) LLA + SF with $G_{ggg} = G_{q\bar{q}g}$, where G_{ggg} and $G_{q\bar{q}g}$ are the coupling constants.

Model 1) gives a distribution of $r(x)$ slightly decreasing as x increases, while model 2) (which is the LUND MC) gives a flat distribution. The difference is due to the fact that the energy dependence of the fraction of multi-parton events is stronger in model 1) than that in model 2). When partons are produced with fixed y, the fraction of events with a given number of partons is almost energy independent, while, when produced with m fixed, the fraction of events with multiple partons increases as E_{CM} increases. Model 3) (which is the Webber MC) and model 4) give almost the same result, and are consistent with data. The comparison between model 3) and model 4) shows that the ratio $r(x)$ is insensitive to the models of the hadronization, despite the fact that the spectrum itself depends on the hadronization model (see Sec.2.2). Model 5), in which less gluons are emitted than model 4), gives a slightly decreasing distribution, but the decrease is weaker than that of Model 4). The conclusion from these studies

is that more partons are required than is provided by a model based on 2nd order QCD.

6 Analysis of 3 jet events

In this section, 1) the string effect in 3 jet events and 2) the dependence of this effect on particle momentum are discussed. IF and SF models are tested to see whether they can explain the measured effect. Data are also compared with LLA based CF models and the soft gluon interference effect is discussed.

6.1 String effect in 3 jet events

The string effect was first observed by JADE.[50] TPC[51] and TASSO[52] have confirmed this effect. The analysis was done as follows (Fig.16):

- Particles were projected into the event plane.
- 3 Jet events were selected by Sphericity cuts (except for TASSO), and by the clustering algorithm or by the generalized sphericity method.
- The momentum of each jet was calculated by summing vector momenta of particles in the jet, while the energy of each jet was calculated by the opening angles between jets.
- The largest energy jet and the smallest energy jet are called jet 1 and 3, respectively. The probability that jet 3 is the gluon jet was estimated to be around 50% based on a Monte Carlo study.
- Using these 3 jet samples, the following quantities were studied;

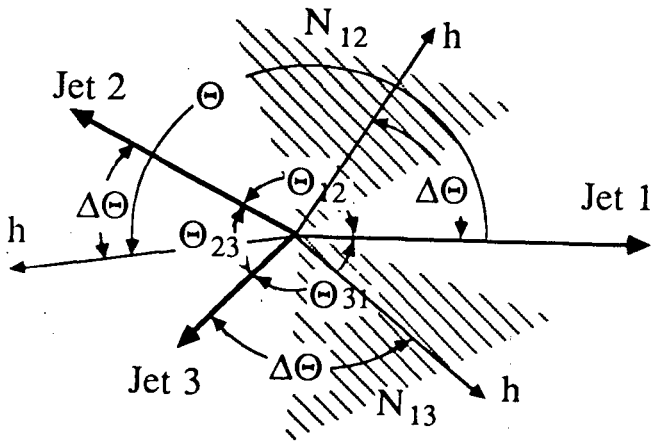

Fig. 16. Definitions of variables in the analysis of 3 jet events.

1. The particle and energy flow in the event plane.
2. The mass and P_{out} dependence of N_{13}/N_{12}. Here N_{ij} is the number of particles between jet i axis and jet j axis with $\Delta\Theta = 0.3 - 0.6 \times \Theta_{ij}$ $(0.25 - 0.75$ for TASSO) and $\Delta\Theta$ is the angle between jet i axis and particle and Θ_{ij} is the angle between jet i axis and jet j axis.
3. The dependence of N_{13}/N_{12} on the probability of jet 3 being the gluon jet.

Figure 17(a) and (b) show the heavy particle flow by TPC and the energy flow by JADE in the event plane as a function of Θ. Here Θ is the angle of particles in the event plane measured from the direction of jet1 through jet2 to jet3. In Fig.18, N_{13}/N_{12} reported by TPC, JADE and TASSO are plotted for particles with different masses and with different P_{out}, the momentum component out of the event plane. It is clear from Fig.18 that the ratio is larger than unity and more hadrons are produced between jet 1 - jet 3 (quark-gluon) than between jet 1 - jet 2(quark-antiquark). The ratio N_{13}/N_{12} is larger for heavier particles and for particles with larger P_{out}.

In Fig.17 and 18, the predictions by the LUND, Hoyer, Webber and Gottschalk models are also given. The Hoyer and Gottschalk models predict the ratio N_{13}/N_{12} to be unity, independently of hadron mass and P_{out}. This prediction is common for all IF based models.[50,51] The LUND and Webber models predict N_{13}/N_{12} to be larger than one and to become even larger for heavier particles or larger P_{out}. These predictions are consistent with experiment data.

In order to confirm that this effect is due to the gluon emission, the ratio N_{13}/N_{12} is plotted as a function of the probability that the jet3 is the gluon jet by TPC[51] (Fig.19). In this analysis, the probability was calculated as follows. The cross section for $q\bar{q}g$ in 1st order QCD is proportional to $C_{q\bar{q}g}$, where

$$C_{q\bar{q}g} = (x_q^2 + x_{\bar{q}}^2)/(1 - x_q)(1 - x_{\bar{q}}),$$

and x_q and $x_{\bar{q}}$ are the energy fractions of the quark and antiquark. The probability G_{tag}(jet3) is defined as

$$G_{tag}(jet3) = 100 \times C_3/(C_1 + C_2 + C_3),$$

where C_i is the value of $C_{q\bar{q}g}$ when jet i is the gluon jet, using the experimentally determined jet energies. It is clear from this figure that the string effect is enhanced for those events with a higher probability G_{tag}(jet3). The difference between the IF model prediction and the LUND and Webber model predictions are enhanced for those events.

Two different models, LUND and Webber, reproduce the string effect, including the mass and P_{out} dependences of the effect. The common characteristic

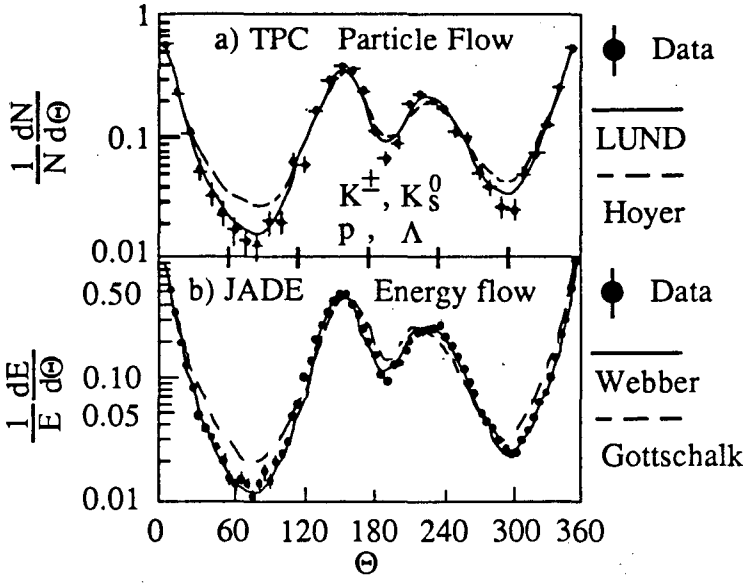

Fig. 17. (a) Heavy particle flow by TPC and (b) Energy flow by JADE in 3 jet events. Monte Carlo predictions are also given.

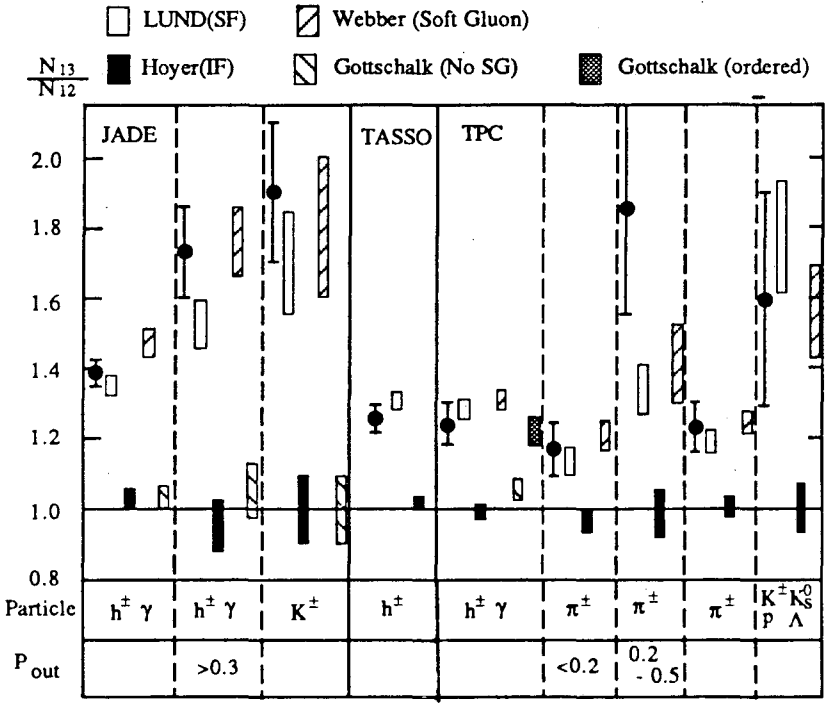

Fig. 18. The ratios N_{13}/N_{12} for different masses and P_{out} of particles. Several MC predictions are also shown. The MC prediction marked by a gray box given by TPC is the Gottschalk MC prediction using only those events in which the angles of partons are ordered (see text).

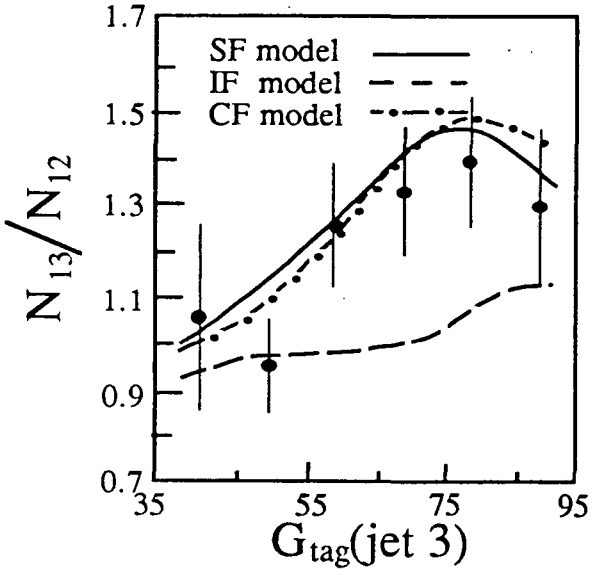

Fig. 19. The ratio N_{13}/N_{12} as a function of the probability that jet3 is the gluon jet, $G_{tag}(jet3)$, measured by TPC.

of these two models is that hadrons are produced from sources moving towards between $q-g$ or between $\bar{q}-g$ in the e^+e^- CM frame. The invariant mass of the source of hadrons depends on the cutoff value of the perturbative phase. The average string mass in the LUND model in the 3 jet sample is around 6 GeV, while the average cluster mass in the Webber model is about 2 GeV; nevertheless both models provide similar predictions for N_{13}/N_{12}.

The soft gluon interference effect, a part of the next to leading order correction, becomes important in the perturbative phase of QCD.[19] Interference terms due to multi-soft gluon emissions cancel a part of the LLA cross section. This effect can be approximately incorporated in Monte Carlo programs by requiring the angles between partons to be ordered, i.e., $\theta_1 > \theta_2$, where θ_1 is the angle between partons preceeding the partons with opening angle of θ_2.[15]

In the Webber model, the angular ordering between partons ensures that partons are more likely to be produced along the direction of the parent parton. This causes depletion of partons between the quark and antiquark jets and depletion of clusters between the quark and antiquark jets. To confirm this point, the ratio N_{13}/N_{12} was calculated using the Gottschalk model, in which soft gluon interference is not included. The Gottschalk model predicts $N_{13}/N_{12} = 1.03 \pm 0.03$. If one uses, however, only those events in which the angles between partons are accidentally ordered, the ratio becomes $N_{13}/N_{12} = 1.22 \pm 0.04$ (See Gottschalk MC predictions in TPC analysis in Fig.18).

6.2 SF vs IF for large momentum particles

The analysis presented above is sensitive to the distribution of hadrons in the central region, which primarally contains small momentum hadrons. TASSO has observed a reversal of the string effect for high momentum particles in

the regions between jets, however, i.e., the IF model seems to be favored over SF.[52] Other groups, JADE[53] and TPC[54], have also examined high momentum particles. Neither of them confirmed the above TASSO result.

TASSO has analyzed the data with two methods:

i. The x_{in} dependence of the N_{13}/N_{12} ratio.

ii. The power dependence of the N_{13}/N_{12} ratio.

In the first analysis, the N_{13}/N_{12} ratio was plotted as a function of x_{in}, where $x_{in} = p_{in}/E_{beam}$ and p_{in} is the particle momentum projected onto the event plane. The data is shown in Fig.20(a) and (b). TASSO has observed that the data points deviate from the prediction of the SF model in the region of $x_{in} > 0.4$, but are consistent with the IF model. The deviation is enhanced when low planarity events are selected, where planarity P is defined to be $P = Q_2 - Q_1$ and Q_2 and Q_1 are medium and smallest eigenvalues of the sphericity tensor. The TPC and JADE data analyzed in an analogous fashion are shown in Fig.20(c) to (e). As can be seen from these figures, the TPC and JADE data are consistent with the SF model predictions at both large and small x_{in} values.

The second analysis by TASSO was done using charged particles as:

- Three jet events are selected by the generalized sphericity technique and by requiring that the opening angle between any two jets be larger than 55°.

- The jet axis is then defined by calculating momentum weighted vector sum

$$\hat{k}_j(n) \propto \sum |p_{in}|^{n-1} \overrightarrow{p}_{in},$$

  where the sum runs over the tracks associated with jet j. The jet axis is determined mainly by small momentum particles for small power of n and by large momentum particles for large power of n.

- For each power of n, the scaled energy of each jet is calculated by the opening angle between jets, and the jets are labeled 1, 2 and 3 in decreasing order of energy.

- The transverse momentum of jet 3 with respect to jet 1 direction is defined to be $x_T(n)$. The difference $\Delta x_T(n) = x_T(2) - x_T(n)$ is used to study the momentum dependence of $x_T(n)$.

Figure 21(a) shows the average value of $x_T(n)$ as a function of n. JADE analyzed data in an analogous fashion using charged particles and photons as shown in Fig.21(b). While TASSO did not impose the planarity cut, JADE

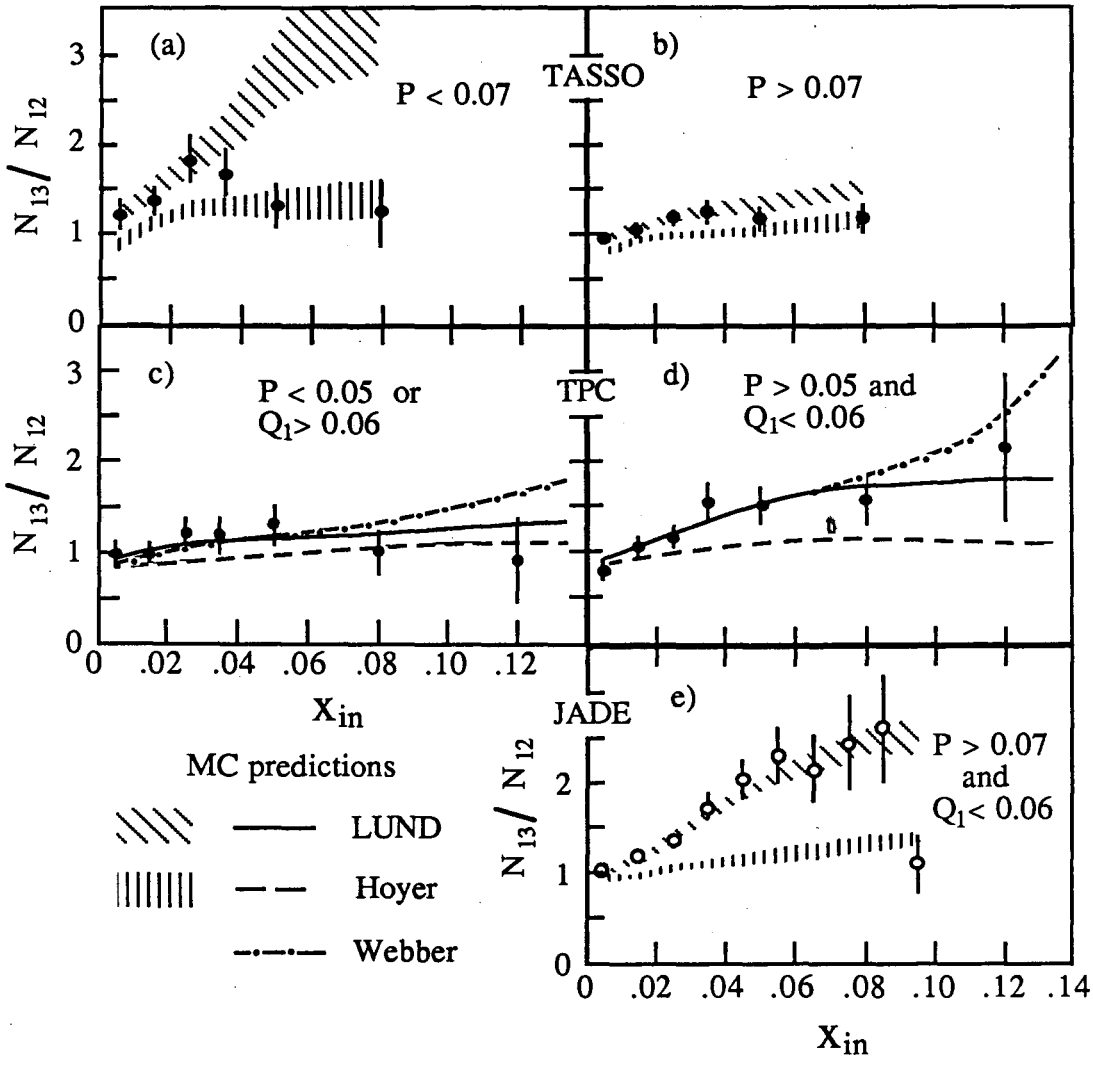

Fig. 20. The ratio N_{13}/N_{12} as a function of x_{in} by TASSO, TPC and JADE. Ranges of P and Q_1 used to select events are shown in the figure. Data are compared with MC predictions.

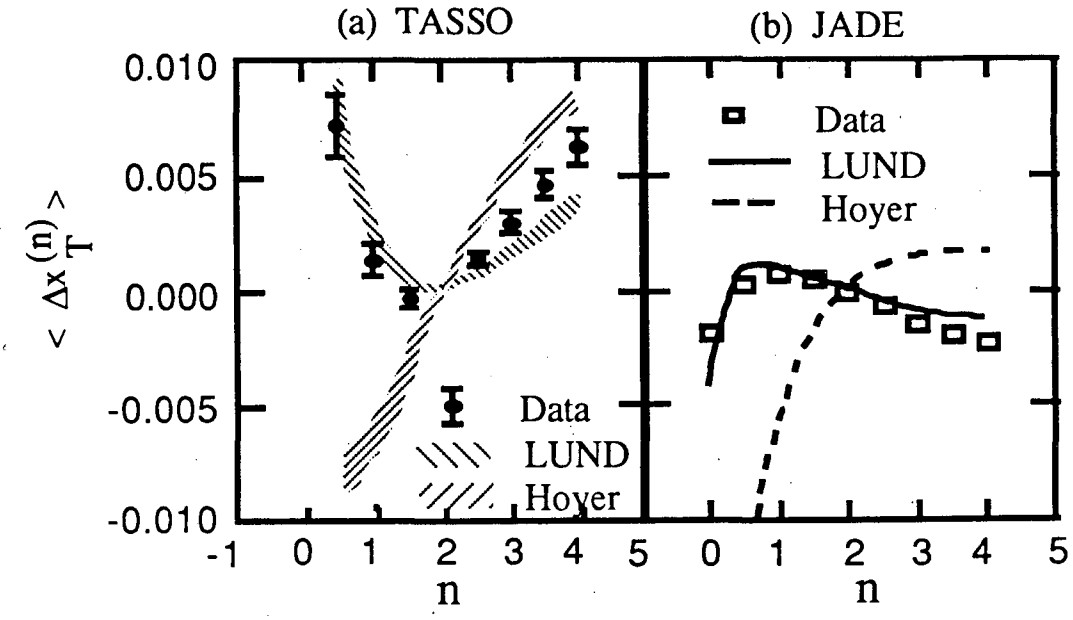

Fig. 21. The difference $\Delta x_T(n)$ as a function of the power n measured by TASSO (a) and by JADE (b).

required planarity cut ($P > 0.07$) and aplanality cut($Q_1 < 0.06$). In order to reduce the difference between TASSO and JADE analyses, events containing more than 3 jets are removed from TASSO data using the clustering algorithm for this plot. The distribution of $\Delta x_T(n)$ is strongly dependent on the analysis, and therefore the n dependence is different from analysis to analysis. In the low n region, the two analyses are in agreement that SF is better than IF. But in the higher n region, the two analyses give different results. The TASSO data points come closer to the prediction of IF for high n region, while the JADE data still favor SF.

The high momentum region is very sensitive to the heavy quark production and the parton production cross sections. More data and further analyses would helpf to settle the discrepancy between TASSO on the one hand and JADE and TPC on the other.

7 Strong Coupling Constant α_S

The measurement of α_S have been done by comparing various measured distributions with predictions of Monte Carlo based on 2nd order QCD and SF or IF hadronization models. These measurements on α_S at PEP and PETRA are summarized in Fig.22.[55] The results on α_S are grouped into three, those determined by the SF model, those by the IF model and those which were found to be insensitive to the hadronization model.

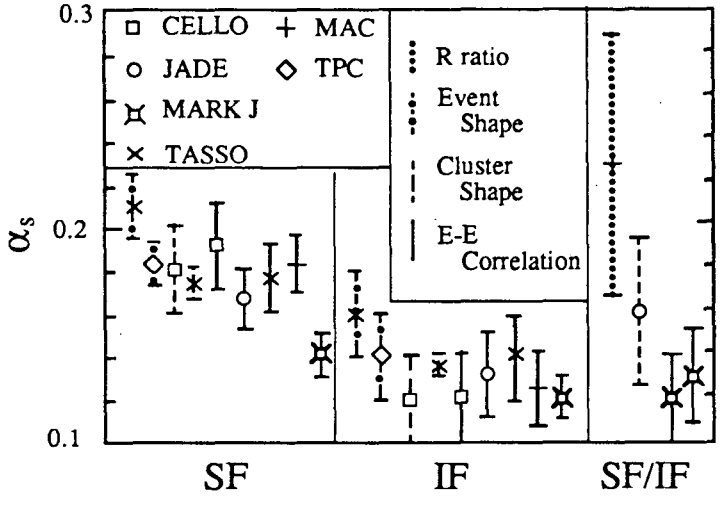

Fig. 22 Strong coupling constant α_s measured by PEP and PETRA experiments.

Four types of methods are used to extract α_S from data:

1) R ratio : the ratio of the total hadronic cross section to the $e^+e^- \rightarrow \mu^+\mu^-$ cross section.

2) Event Shape : quantities based on particle distributions, e.g., p_t and sphericity distributions.

3) Cluster Distribution : quantities based on cluster distributions, e.g., sphericity calculated using reconstructed cluster momentum.

4) Energy-Energy correlation : correlations between the energy flow of particles defined as

$$\frac{1}{\sigma}\frac{d\Sigma}{d\cos\xi} = \frac{1}{N}\sum_{event}^{N}\sum_{i,j}\frac{E_iE_j}{E_{vis}^2}\delta(\cos\xi_{ij} - \cos\xi),$$

where E_i is the energy of particle i and ξ_{ij} is the spatial angle between particle i and j.

Duke and Roberts[3] calculated a world average of α_S to find $\alpha_S = 0.19 \pm 0.06$ at $< E_{CM} >= 34.2\ GeV$ and $\Lambda_{\overline{MS}} = 880^{+1360}_{-740}\ MeV$.

There exits two types of analysis dependence among measured values of α_S. One comes from the fact that the value of α_S extracted from data depends heavily on the hadronization model used in the analysis. From same data, one gets larger α_S by using the SF model than by using the IF model. It

has been proven that the smaller value of α_S obtained with IF is not due to the momentum conservation scheme nor due to the treatment of the gluon fragmentation.[55] The second discrepancy is that the value of α_S reported by MARK J using the SF model is smaller than the values by other groups. This difference originates from the different treatment of the regularization of the parton cross section. The R ratio is least sensitive to the hadronization model, but the value of α_S is extracted from the small correction term, $R \propto 1 + \alpha_S/\pi$, and the measurement is very difficult.

Many suggestions have been made to resolve these discrepancies, but no definitive scenario has yet been given.[3,5,55] In the following, listed are some key points which might help to settle these discrepancies:

1. Dependence on the hadronization model : the analysis of 3 jet events (Section 6.1) has shown that the IF model cannot describe the hadron distribution in the central rapidity region. The determination of α_S using the IF model must be done in such a way that the result is insensitive to the hadron distribution in this region.

2. Definition of dressed parton : it has been pointed out that the definition of dressed partons in the calculation of the 2nd order QCD cross sections may affect the determination of α_S at the level of 10 %.[56] Therefore quantitative studies are required to see how α_S is really affected.

3. Effects of higher order corrections : it has been proven that the 2nd order cross sections currently used by the SF and IF models may not be adequate 1) from the study of the fraction of 4 jet events[57] and 2) by the analysis of 3 jet events by MARK II (Section 5.2)[49]. The determination of α_S must be done in such a way that the effects due to higher order is small. In the determination of $\alpha_S(Q^2)$ or $\Lambda_{\overline{MS}}$ including the higher order terms, Monte Carlo programs based on LLA are not useful. In order to obtain $\Lambda_{\overline{MS}}$ using MC's based on the renormalization group, next to leading order must be fully taken into account.

8 Forward-Backward asymmetry of Quarks and Leptons

The test of the Weinberg-Salam model has been done by studying the forward-backward asymmetry in $e^+e^- \rightarrow q\bar{q}, \ell\bar{\ell}$. In the following, the measured values of the weak axial coupling constant g_f are summaried, where f represents μ, τ, c or b. In the derivation of these results, the theoretical value of $g_e = -1/2$ is used, which is consistent with the measured results.[58,60]

Table 2 gives a summary of the recent measurements on the weak axial coupling constants from the F-B asymmetry of leptons. Old data are included for completeness.[61] In the same table, the world average for g_μ and g_τ are also shown. The data are consistent with the prediction of the W-S model $g_\ell = -1/2$.

The F-B asymmetry of quarks was measured using 1) prompt muons, 2) prompt electrons and 3) D and D*.[62] New results since the Leipzig Conference have been reported by HRS and TPC. Their data and the world average presented at the Cornell and Leipzig conferences are shown in Table 2. The value of g_Q is quite consistent with the theoretical prediction $g_c = +1/2$ and $g_b = -1/2$ for both the bottom and charm quarks.

μ		τ	
g_μ	Collaboration	g_τ	Collaboration
-0.55±0.18	CELLO	-0.46±0.16	CELLO
-0.65±0.085	JADE	-0.37±0.11	JADE
-0.69±0.10	MARK J (34.6GeV)	-0.48±0.27	MARK J
-0.52±0.13	MARK J (44.6GeV)		
-0.705±0.165	PLUTO	-0.31±0.38	PLUTO
-0.52±0.12	TASSO (34.5GeV)	-0.26±0.34	TASSO
-0.60±0.16	TASSO (43.69GeV)		
-0.416±0.135	HRS	-0.56±0.23	HRS
-0.50±0.06	MAC	-0.44±0.10	MAC
-0.64±0.14	MARK II	-0.38±0.18	MARK II
-0.57±0.03	World Ave	-0.42±0.06	World Ave
charm quark		*bottom quark*	
g_c	Collaboration	g_b	Collaboration
0.61±0.2	Av(PETRA) 83	-0.50±0.15	Av(PETRA) 83
0.50±0.20	Av(PETRA) 84	-0.47±0.11	Av(PETRA) 84
1.2±0.8	Av(PEP) 83	-0.55±0.25	Av(PEP) 83
0.60±0.15	Av(PEP) 84	-0.57±0.12	Av(PEP) 84
0.6±0.4	HRS($D^{*\pm}$)		
0.74±0.27	HRS($D^{*\pm}$,D)		
1.15±0.86	TPC(e)	-1.0±0.98	TPC(e)
0.75±0.79	TPC(μ)	-0.45±0.57	TPC(μ)
0.89±0.92	TPC($D^{*\pm}$)		
0.61±0.15	World Ave	-0.49±0.10	World Ave

Table 2. Weak axial coupling constant for fermions. In the table, Av(PETRA,PEP) 83 and 84 means the average of values for PETRA and PEP experiments presented in Cornell[59] and Leipzig[60] conferences, respectively. The world average are calculated from the values listed in this table.

9 Summary

In this presentation recent results on hadron production in e^+e^- annihilations have been summarized with an emphasis on the hadron production mechanism.

In order to understand the hadronization process in the framework of QCD, the questions which need to be answered are 1) how the perturbative phase merges with the non-perturbative phase and 2) how partons in the non-perturbative phase transform into hadrons. The data have been compared with predictions of models based on different assumptions and calculations. For the perturbative phase, parton cross sections are calculated based either on 2nd order QCD or on LLA, possibly with a part of the corrections from the next to leading log. For the non-perturbative phase, hadronization models tested are the independent fragmentation model(IF), the string fragmentation model(SF) or the cluster fragmentation model (CF).

The measurement of the strong coupling constant α_S in the jet production process still contains ambiguities, and specific points where further study is required are pointed out.

The gluon jet study by MARK II has shown that the particle spectrum in gluon jets is softer than that in quark jets. By comparing the data with the predictions of several Monte Carlo programs, multigluon emission is found to make the spectrum soft. In this case, LLA is a better approximation than the 2nd order QCD.

The flavor dependence of the hadronization process is studied by using charm and bottom enriched events tagged by prompt leptons and D*. Available data are consistent with the QCD prediction that hadronization is independent of the quark flavor. Apparent differences in data between heavy quark jets and light quark jets are explained by differences in the momentum spectrum and decay of the first rank hadron.

Cross sections for many kinds of hadrons are fairly well reproduced by a model based on LLA and CF hadronization with only a few fundamental parameters to be adjusted. The SF model, which is very successful in describing hadronization, cannot predict the multiplicities without adjusting several phenomenological parameters. HRS measured the inclusive particle cross section up to $z = 1$. The data are inconsistent with the prediction of the CF model in the region above z = 0.6. Another problem with the CF model is its isotropic cluster decay mechanism as has been pointed out by TPC in $p - \overline{p}$ correlation studies. These problems originate from a simplified treatment of the cluster fragmentation model.

The 3 jet event analysis has proven that the IF model cannot explain the depletion of soft hadrons in the region between the quark and antiquark directions. The SF model explains this signal by the absence of a string between the

quark and antiquark. The model with LLA and CF also explains this "string effect" mainly by the soft gluon interference effect. TASSO has reported that the IF model is favored for high momentum hadrons in the region between $q-\overline{q}$. JADE and TPC do not observe this effect, however. Further study is required to determine whether the SF model can reproduce particle distributions in the entire momentum range.

The $p-\overline{p}$ correlation studied by TPC has given the following two results. The observed $p-\overline{p}$ correlation in the polar angle is consistent with the diquark and popcorn mechanisms in the SF model but not consistent with the spherically symmetric decays of clusters incorporated in the CF model. The $p-\overline{p}$ correlation in azimuthal angle is relatively weak, suggesting that a meson pops up between a baryon antibaryon pair at least a half of time.

The couplings of fermions and Z^0 measured by the forward-backward asymmetries of leptons and quarks are consistent with the predictions of the Weinberg-Salam model.

Acknowledgements

I would like to thank groups who provided new results prior to publication. I am indebted for stimulating discussions by H.-U. Bengtsson, J. Dorfan, J. W. Gary, W. Hofmann, P. Kooijman, A. Petersen, T. Sjoestrand, K. Sugano, and B. R. Webber. T. Kamae, P. Oddone, H. Aihara and E. Wang and other colleagues in the PEP4/TPC collaboration constantly encouraged me in the preparation of the talk and corrected my English in this manuscript. I would also like to express my gratitude to the organizing committee and the program committee for providing me the chance to give this talk.

References

1. See, for example, E. Reya, Phys. Rep. 69 (1981) 195; A. H. Muller, Phys. Rep. 73 (1981) 237; G. Altarelli, Phys. Rep. 81 1.

2. A. H . Muller, talk at this meeting.

3. D. W. Duke and R. G. Roberts, Phys. Rep. 120 (1985) 276.

4. S. Glashow, Nucl. Phys. 22 (1961) 579; S. Weinberg, Phys. Rev. Lett. 19 (1967) 1264; A. Salam, Proceedings of the Eighth Nobel Symp. (Almqvist and Wiksells, Stockholm, 1968), p.367.

5. See, for example, J. Dorfan, Proc. of the 1983 Int. Symp. on Lepton and Photon Interactions at High Energies, Cornell University, Aug.

4-9, 1983, p686; W. Hofmann, Proc. of the Symp. on the High Energy e^+e^- Interactions, Vanderbilt, Tennessee, Apr. 5-7, p329.

6. S. L. Wu, Phys. Rep. 107, 59 (1984).

7. R. K. Ellis, D. Ross and A. Terrano, Phys. Lett. 45B (1980) 1226; Nucl. Phys. B178 (1980) 421; K. Fabricius, G. Kramer, G. Schierholz and I. Schmitt, Phys. Lett. 97B (1980) 431; Z. Phys. C11 (1982) 315; J. Vermaseren, J. Gaemers and S. Oldham, Nucl. Phys. B187 (1981) 301; A. Ali and F. Barreiro, Phys. Lett. B118 (1982) 155; Nucl. Phys. B236 (1984) 269; F. Gutbrod, G. Kramer and G. Schierholz, Z. Phys. C21 (1984) 235.

8. S. Wolfram, XV Recontre de Moriond (1980); R. Odorico, Nucl. Phys. B172 (1980) 157; Phys. Lett. 102B (1981) 341; P. Mazzanti and R. Odorico, Phys. Lett. 95B (1980) 133; Z. Phys. C7 (1980) 61; See also Ref.14, 15 and 16.

9. See, for example, R. D. Field, Proc. of the 1983 Int. Symp. on Lepton and Photon Interactions at High Energies, Cornell University, Aug. 4-9, 1983, p593; T. D. Gottschalk, Lectures at the 19th Int. School of Elementary Particle Physics, Kupari-Dubrovnik, Yugoslavia, 1983.

10. R. Field and R. Feynman, Nucl. Phys. B136 (1978) 1.

11. A. Ali et al., Phys. Lett. B93 (1980) 155.

12. P. Hoyer et al., Nucl. Phys. B161 (1979) 349.

13. B. Andersson et al., Phys. Rep. 97 (1983) 31; T. Sjoestrand, Com. Phys. Comm. 27 (1982) 243; 28 (1983) 229.

14. G. C. Fox and S. Wolfram, Nucl. Phys. B168 (1980) 285; R. D. Field and S. Wolfram, Nucl. Phys. B213 (1983) 65.

15. G. Marchesini and B. R. Webber, Nucl. Phys. B238 (1984) 1; B. R. Webber, Nucl. Phys. B238 (1984) 492.

16. T. D. Gottschalk, Nucl. Phys. B214 (1983) 201; B239 (1984) 325; B239 (1984) 349.

17. T. Sjoestrand, Phys. Lett. 142B (1984) 420.

18. Some problems of the CF model are discussed in T. D. Gottschalk and M. Derrick, Proc. of the 1984 Summer Study on the Design and Utilization of the Superconducting Super Collider, Snowmass, CO (1984).

19. A. H. Muller, Phys. Lett. 104B (1981) 161; Yu. L. Dokshitzer, V. S. Fadin and V. A. Khoze, Phys. Lett. 115B (1982) 242; L. V. Gribov, E. M. Levin and M. G. Ryskin, Phys. Rep. 100 (1983) 1; A. Bassetto, M. Ciafaloni and G. Marchesini, Phys. Rep. 100 (1983) 201; R. Odorico, paper 346 submitted to this conference.

20. $\pi^{\pm}$ PEP4/TPC Collab., H. Aihara et al., Phys. Rev. Letter 52 (1984) 577; TASSO Collab., paper 399 submitted to this conference; HRS Collab., M. Derrick et al., ANL-HEP-PR-85-69, PU-85-537, IUHEE-69, UM HE 85-16 (1985);
π^0 TASSO Collab., R. Brandelik et al., Phys. Lett. 108B, (1982) 71; CELLO Collab., H.J. Behrend et al., Z. Physik C20 (1983) 207; PEP4/TPC Collab., H. Aihara et al., Z. Physik C27, 187 (1985); JADE Collab., W. Bartel et al., DESY 85-029 (Apr. 1985);
ρ^0 TASSO Collab., R. Brandelik et al., Phys. Lett. 117B (1982) 135; JADE Collab., W. Bartel et al., Phys. Lett. 145B (1984) 441; MARK II Collab., H. Schellman et al., SLAC-PUB-3448, LBL-18391 (Sep. 1984); HRS Collab., M. Derrick et al., ANL-HEP-PR-85-20, PU-85-527, IUHEE-65, UM-HE-85-10 (1985);
$K^{\pm}$ PEP4/TPC Collab., Ref. for $\pi^{\pm}$; MARK II Collab., H. Schellman et al., Phys. Rev. D31 (1985) 3013; TASSO Collab., Ref. for $\pi^{\pm}$; HRS Collab., Ref. for $\pi^{\pm}$;
K^0_S JADE Collab., W. Bartel et al., Z. Physik C20 (1983) 187; PEP4/TPC Collab., H. Aihara et al., Phys. Rev. Lett. 53 (1984) 2378; TASSO Collab., M. Althoff et al., Z. Physik C27, (1985) 27; MARK II Collab., Ref. for $K^{\pm}$; HRS Collab., Ref. for $\pi^{\pm}$;
K^{*0} PEP4/TPC Collab., Ref. for K^0_S; MARK II Collab., Ref. for ρ^0; HRS Collab., Ref. for ρ^0;
$K^{*\pm}$ JADE Collab., Ref. for ρ^0; MARK II Collab., Ref. for ρ^0;
ϕ PEP4/TPC Collab., H. Aihara et al., Phys. Rev. Lett. 52 (1984) 2201; HRS Collab., M. Derrick et al., Phys. Rev. Lett. 54 (1985) 2568;
η JADE Collab., Ref. for π^0;
p PEP4/TPC Collab., Ref. for $\pi^{\pm}$; TASSO Collab., Ref. for $\pi^{\pm}$;
Λ JADE Collab., W. Bartel et al., Phys. Lett. 104B (1981) 325; PEP4/TPC Collab., H. Aihara et al., Phys. Rev. Lett. 54 (1985) 274; TASSO Collab., Ref. for K^0_S; MARK II Collab., C. de la Vaissiere et al., Phys. Rev. Lett. 54 (1985) 2071; HRS Collab., Ref. for $\pi^{\pm}$;
Ξ^- PEP4/TPC Collab., K. Maruyama, XIX Recontre de Moriond (1984); TASSO Collab., Ref. for K^0_S;
Δ^{++} TASSO Collab., M. Althoff et al., DESY 84-065 (Jul. 1984);
$\Sigma^{*\pm}$ TASSO Collab., Ref. for Δ^{++}; PEP4/TPC Collab., Collab., H.

Yamamoto, XX Recontre de Moriond (1985);
Ω^- TASSO Collab., LUND Conference (1984); PEP4/TPC Collab., Ref. for $\Sigma^{*\pm}$.

21. ARGUS Collab., R. S. Orr, EPS Meeting on HEP, Bari, Italy, Jul. 1985.

22. MARK II Collab., H. Schellman et al., Phys. Rev. 31 (1985) 3013; See also Ref. 20.

23. B. Andersson, G. Gustafson and B. Soederberg, Z. Phys. C20 (1983) 317.

24. HRS Collab., M. Derrick et al., ANL-HEP-PR-85-77 (1985).

25. T. D. Gottschalk, private communication.

26. DELCO Collab., H. Yamamoto et al., Phys. Rev. Lett. 54 (1985) 522 and references therein; PEP4/TPC Collab., H. Aihara et al., IS-J-1848.

27. MARK III Collab., A. Duncan, SLAC Summer Inst. on Particle Physics, Jul. 29 - Aug. 6, 1985.

28. Particle Data Group, Rev. Mod. Phys. 56 (1984) No.2.

29. S. Bethke, paper 325 submitted to this conference.

30. CLEO Collab., T. Bowcock et al., Phys. Rev. Lett. 55 (1985) 923.

31. MARK II Collab., G. S. Abrams et al., Phys. Rev. Lett. 44 (1980) 10;

32. C. Peterson et al., Phys. Rev. D27 (1983) 105.

33. MARK II Collab., M. E. Nelson et. al., Phys. Rev. Lett. 50 (1983) 1542; N. S. Lockyer et al., Phys. Rev. Lett. 51 (1983) 1316.

34. MAC Collab., E. Fernandez et al., Phys. Rev. Lett. 50 (1983) 2054; MARK J Collab., B. Adeva et al., Phys. Rev. Lett. 51 (1983) 443; TASSO Collab., M. Althoff et at., Z. Phys. C22 (1984) 219; DELCO Collab., T. Pal et al., CALT-68-1283 (1985).

35. HRS Collab., M Derrick et al., ANL-HEP-PR-85-47 (1985).

36. DELCO Collab., M. Sakuda et al., Phys. Lett. 152B (1985) 399.

37. TASSO Collab., M. Althoff et al., Phys. Lett. 138B (1984) 317.

38. JADE Collab., W. Bartel et al., Phys. Lett. 146B (1984) 121.

39. HRS Collab., P. R. Keston, PhD Thesis in The University of Michigan (1985).

40. G. Goldhaber, 1st Int. Workshop on Local Equilibrium in Strong Interaction Physics, Sep. 3-6, 1984; PEP4/TPC Collab., H. Aihara et al., Phys.Rev. D31 (1985) 996; CLEO Collab., P. Avery et al., CLEO-85-3 (1985); TASSO Collab., M. Althoff et al., paper 395 submitted to this conference.

41. PEP4/TPC Collab., H. Aihara et al., Phys. Rev. Lett. 55 (1985) 1047.

42. B. Andersson, G. Gustafson and T. Sjoestrand, Nucl. Phys. B197 (1982) 45; T. Meyer, Z. Phys. C12 (1982) 77.

43. A. Casher, H. Neuberger and S. Nussinov, Phys. Rev. D20 (1979) 179; B. Andersson, G. Gustafson and T. Sjoestrand, LU TP 84-9 (1984).

44. The Webber Monte Carlo[15] is used in their analysis.

45. TASSO Collab., Ref. for K_S^0.

46. MARK II Collab., Ref. for Λ.

47. HRS Collab., P. Baringer, XX Moriond Conference (Mar. 1985);

48. S. Behrends et al., Phys. Rev. D31 (1985) 2161.

49. MARK II Collab., A. Petersen et al., SLAC-PUB-3759 (1985); MARK II Collab., private communication.

50. JADE Collab., W. Bartel et al., Phys. Lett. 101B (1981) 129; Z. Phys. C21 (1983) 37; Phys. Lett. 134B (1984) 275; paper 379 submitted to this conference.

51. PEP4/TPC Collab., H. Aihara et al., Phys. Rev. Lett. 54 (1985) 270; Z. Phys. C28(1985)31.

52. TASSO Collab., M. Althoff et al., paper 400 submitted to this conference

53. JADE Collab., A. Petersen, Private communication.

54. J. W. Gary, PhD Thesis in Lawrence Berkeley Laboratory (1985).

55. CELLO Collab., H.-J.Behrend et al., Phys. Lett. 138B(1984)311; JADE Collab., W.Bartel et al., Phys. Lett. 119B(1982)239; Z. Phys. C25(1984)231; MARK J Collab., B.Adeva et al., Phys. Rev. Lett. 50(1983)2051; Phys. Rev. Lett. 54(1985)1750; TASSO Collab., M.Althoff et al., Z. Phys. C26(1984)157; MAC Collab., E.Fernandez et al., Phys. Rev. D31(1985)1537; Phys. Rev. D31(1985)2724; PEP4/TPC Collab., H.Aihara et al., Z. Phys. C28(1985)31.

56. T. D. Gottschalk and P. Shatz, Caltech preprint CALT-68-1172 (1984); CALT-68-1173 (1984); CALT-68-1199 (1984).

57. TASSO and PEP4/TPC Collab., Ref.'s for α_S.

58. PLUTO Collab., Ch. Berger et al., Z. Phys. C27 (1985) 341.

59. B. Naroska, Proc. 1983 Int. Symp. Lepton-Photon Int. at High Energies (Cornell 1983) p96.

60. P. Langacker, Proc. 22nd Int. Conf. H. E. Phys. (Leipzig) Vol. 2, p91; R. Prepost, Vol. 1, p227; C. K. Bowdery, Vol. 1, p229; E. Wicklund, Vol. 1, p230.

61. CLLEO Collab., paper 258 submitted to this conference; JADE Collab., W. Bartel et al., Z. Phys. C26 (1985) 507; W. Bartel et al., DESY 85-065 July 1985; MARK J Collab., B. Adeva et al., Technical Report Number 144, March, 1985; B. Adeva et al., Phys. Rep. 109 (1984) 131; PLUTO Collab., Ch. Berger et al., Z Phys. C21 (1983) 53; Ch. Berger et al., DESY 85-017 Feb 1985; TASSO Collab., M. Althoff et al., Z Phys. C22 (1984) 13; paper 397 submitted to this conference; M. Althoff et al., Z. Phys. C26 (1985) 521; HRS Collab., M. Derrick et al., PR D31 (1985) 2352; K. K. Gan et al., Phys. Lett. 153B (1985) 116; MAC Collab., W. W. Ash et al., paper 393 submitted to this conference; E. Fernandez et al., Phys. Rev. Lett. 54 (1985) 1620; MARK II Collab., M. E. Levi et al., Phys. Rev. Lett. 51 (1983) 1941.

62. HRS Collab., M. Derrick et al., Phys. Lett. 146B (1984) 261; S. Abachi et al., paper 264 submitted to this conference; PEP4/TPC Collab., H. Aihara et al., Z. Phys. C27 (1985) 39; H. Aihara et al., Phys. Rev. D31 (1985) 2719; H. Aihara et al., IS-J-1848.

LAWRENCE BERKELEY LABORATORY
TECHNICAL INFORMATION DEPARTMENT
UNIVERSITY OF CALIFORNIA
BERKELEY, CALIFORNIA 94720